International Symposium on Fractional PDEs: Theory, Numerics and Applications, June 3–5, 2013, Salve Regina University, 100 Ochre Point Avenue, Newport RI 02840

More Optimal Image Processing by Fractional Order Differentiation and Fractional Order Partial Differential Equations

Dali Chen, Dingyu Xue, YangQuan Chen

yqchen@ieee.org, ychen53@ucmerced.edu
ME/EECS/SNRI/UCSolar
MESA LAB, School of Engineering,
University of California, Merced, USA

xuedingyu@ise.neu.edu.cn,
chendali@ise.neu.edu.cn
Information Science and Engineering
Northeastern University
Shenyang 110004, P R China

Who cares?

- Minimal dose biomedical imaging
- More optimal

Strategies for Reducing Radiation Dose in CT (McCollough 2009)
Radiol Clin North Am. 2009 January ; 47(1): 27–40. doi:10.1016/j.rcl.2008.10.006

http://www.eurekalert.org/pub_releases/2013-05/aaft-mdc050113.php

FC for what?

- Better than the best
- New sciences

- Need killing apps.

UCMERCED

MESA LAB

UC Merced

- The Research University of the Central Valley
- Central Located
  - Sacramento – 2 hrs
  - San Fran. – 2 hrs
  - Yosemite – 1.5 hrs
  - LA – 4 hrs
- Surrounded by farmlands and sparsely populated areas

UCMERCED

MESA LAB

UC Merced

- Established 2005
- 1st research university in 21st century in USA.
- 6,000 Undergraduates
- 300 Grads (200+ Ph.D)

- Strong Undergraduate Research Presence (HSI, MSI)

MESA LAB

http://mechatronics.ucmerced.edu

- **Mechatronics, Embedded Systems and Automation**
  - **Backup name: *Mechatronics, Energy Systems and Autonomy***
  - **ASME DED, MESA TC. http://iel.ucdavis.edu/mesa/**
    - **2013 MESA conference: Portland, OR http://www.asmeconferences.org/IDETC2013/**

UCMERCED

MESA LAB

MESA Labs

- Director: Dr. YangQuan Chen
- 4 Ph.D. Students
- 1 MSc student
- 20+ Undergraduates
- 4 Visiting Ph.D. Students
- 2 Visiting Professors
- Short term visiting students
- 3 3D printers

MESA Labs

MESA Research Areas/Strengths

- Unmanned Aerial Systems and UAV-based Personal Remote Sensing (PRS)
- Cyber-Physical Systems (CPS)
- Modeling and Control of Renewable Energy Systems
- Mechatronics
- **Applied Fractional Calculus (AFC)**

Roadmap: More Optimal Image Processing

$u_0 = u + n$; u_0 is the given image; n is the noise.

MAP $\quad \widehat{u} = \arg\max_u p(u|u_0) = \arg\max_u p(u)p(u_0|u)$

Stochastic

$$\min E[u|u_0] = \frac{1}{2}\int_\Omega |\nabla u|^2 dx + \frac{\lambda}{2}\int_\Omega (u-u_0)^2 dx$$

Variation

$-\Delta u + \lambda u = \lambda u_0$ Euler-Lagrange Equation

PDE

$$u_0 = u + \frac{-\Delta u}{\lambda} = u + \omega$$ Detail information

Wavelet

Introduction: Optimal Image Processing

$u_0 = u + n$; u_0 is the given image; n is the noise.

MAP $\quad \widehat{u} = \arg\max_u p(u|u_0) = \arg\max_u p(u)p(u_0|u)$

Stochastic

$$\min E[u|u_0] = \frac{1}{2}\int_\Omega |\nabla u|^2 dx + \frac{\lambda}{2}\int_\Omega (u-u_0)^2 dx$$

Variation

$$-\Delta u + \lambda u = \lambda u_0 \quad \text{Euler-Lagrange Equation}$$

PDE

$$u_0 = u + \frac{-\Delta u}{\lambda} = u + \omega \quad \text{Detail information}$$

Wavelet

Outline

- Fractional Order Image Enhancement
- Fractional Order Image Edge Detection
- Fractional Order Image Denoising
- Fractional Order Image Segmentation
- Fractional Order Optical Flow

Fractional Order Image Enhancement

- Aim of Image Enhancement[1]:
  - Enhance the contrast and detail information
  - Easy for observation
  - Easy for subsequent processing

Problem Description

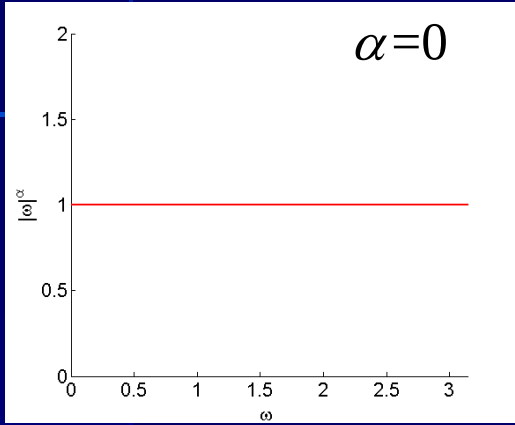

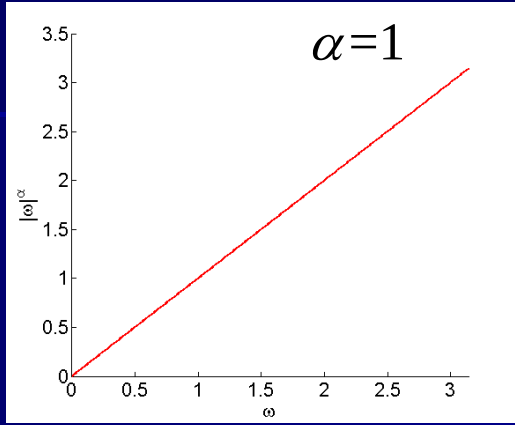

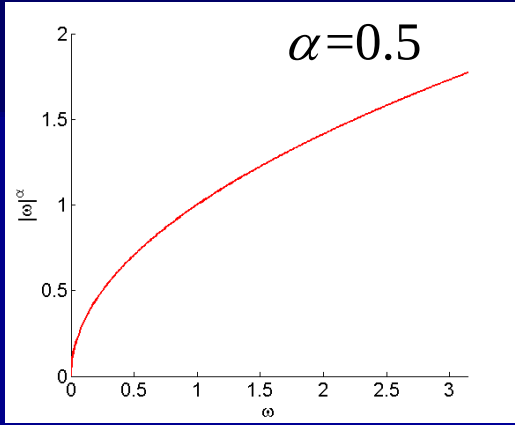

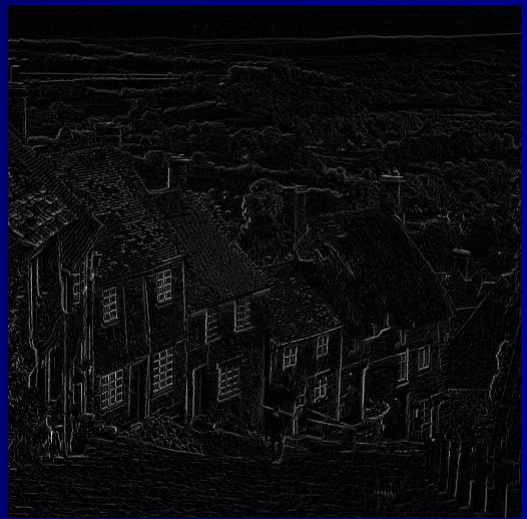

?

Digital Fractional Order Savitzky-Golay Differentiator[2]

$$\widehat{Y_i^{(\alpha)}} = X_i^{(\alpha)} B = W_i^{(\alpha)} Y$$

$$= [\frac{1}{\Gamma(1-\alpha)} i^{-\alpha}, \frac{1}{\Gamma(2-\alpha)} i^{1-\alpha}, \frac{\Gamma(3)}{\Gamma(3-\alpha)} i^{2-\alpha}; \quad (1)$$

$$\ldots, \frac{\Gamma(n+1)}{\Gamma(n+1-\alpha)} i^{n-\alpha}](X^T X)^{-1} X^T Y,$$

Y: input signal;
I: filtering window size;
n: degree of polynomial function;
i = 1,2,...,I.

$$X = \begin{bmatrix} 1 & 1^1 & \ldots & 1^n \\ 1 & 2^1 & \ldots & 2^n \\ \vdots & \vdots & \vdots & \vdots \\ 1 & I^1 & \ldots & I^n \end{bmatrix}$$

Good at dealing with noisy signal

Extend to 2-Dimension[3]

Assume $l=2m+1$ and

$$W_{m+1}^{(\alpha)} = [W(1), W(2), \ldots, W(2m+1)] \tag{2}$$

Then, 2-D DFOSGD templates:

$W_{x+}^{(\alpha)}$

0	0	0	0	0
0		⋮		0
W(1)	⋯	W(m)	⋯	W(2m-1)
0		⋮		0
0	0	0	0	0

$W_{x-}^{(\alpha)}$

0	0	0	0	0
0		⋮		0
W(2m-1)	⋯	W(m)	⋯	W(1)
0		⋮		0
0	0	0	0	0

$W_{y+}^{(\alpha)}$

0	0	W(1)	0	0
0		⋮		0
0	⋯	W(m)	⋯	0
0		⋮		0
0	0	W(2m-1)	0	0

$W_{y-}^{(\alpha)}$

0	0	W(2m-1)	0	0
0		⋮		0
0	⋯	W(m)	⋯	0
0		⋮		0
0	0	W(1)	0	0

Extend to 2-Dimension

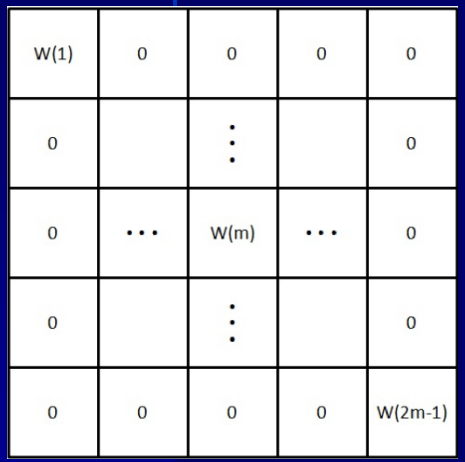

$W^{(\alpha)}_{\searrow}$

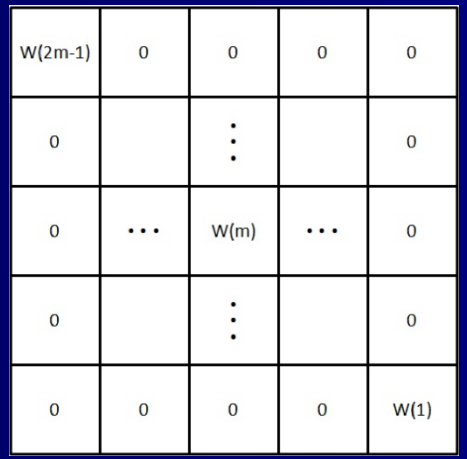

$W^{(\alpha)}_{\swarrow}$

$W^{(\alpha)}_{\nearrow}$

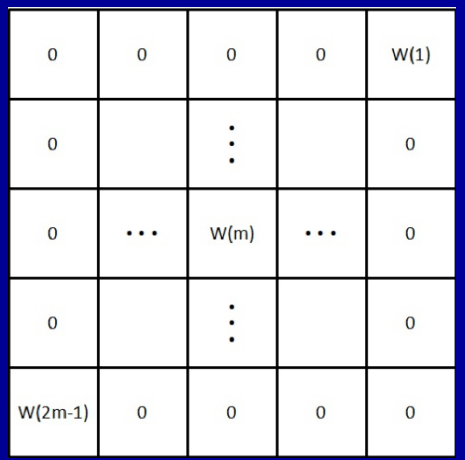

$W^{(\alpha)}_{\nwarrow}$

$$
\begin{aligned}
G_{x^+}^{(\alpha)}(x,y) &= \sum_{k=-m}^{m}\sum_{l=-m}^{m} W_{x^+}^{(\alpha)}(k,l)G(x-k,y-l),\\
G_{x^-}^{(\alpha)}(x,y) &= \sum_{k=-m}^{m}\sum_{l=-m}^{m} W_{x^-}^{(\alpha)}(k,l)G(x-k,y-l),\\
G_{y^+}^{(\alpha)}(x,y) &= \sum_{k=-m}^{m}\sum_{l=-m}^{m} W_{y^+}^{(\alpha)}(k,l)G(x-k,y-l),\\
G_{y^-}^{(\alpha)}(x,y) &= \sum_{k=-m}^{m}\sum_{l=-m}^{m} W_{y^-}^{(\alpha)}(k,l)G(x-k,y-l),\\
G_{\searrow}^{(\alpha)}(x,y) &= \sum_{k=-m}^{m}\sum_{l=-m}^{m} W_{\searrow}^{(\alpha)}(k,l)G(x-k,y-l),\\
G_{\nwarrow}^{(\alpha)}(x,y) &= \sum_{k=-m}^{m}\sum_{l=-m}^{m} W_{\nwarrow}^{(\alpha)}(k,l)G(x-k,y-l),\\
G_{\nearrow}^{(\alpha)}(x,y) &= \sum_{k=-m}^{m}\sum_{l=-m}^{m} W_{\nearrow}^{(\alpha)}(k,l)G(x-k,y-l),\\
G_{\swarrow}^{(\alpha)}(x,y) &= \sum_{k=-m}^{m}\sum_{l=-m}^{m} W_{\swarrow}^{(\alpha)}(k,l)G(x-k,y-l).
\end{aligned}
\tag{3}
$$

Calculate the αth order derivatives of G(x, y) in the different directions by Eq. (3).

G: input image;

Implementation

Image enhancing algorithm flow

- Step 1: Calculate:

$$G_d^{(\alpha)}(x,y),\ d \in \Omega,\ \Omega := \{x^+, y^+, x^-, y^-, \searrow, \nwarrow, \nearrow, \swarrow\}$$

- Step2: Calculate:

$$G^{(\alpha)}(x,y) = Sat(\max\{G_d^{(\alpha)}(x,y) | d \in \Omega\}),$$

Enhanced image

$$Sat(u) = \begin{cases} 0, & u < 0 \\ u, & u \in [0, L], \\ L, & u > L \end{cases}$$

Experiments

Lake Tahoe

http://earthobservatory.nasa.gov/

Snow-covered volcanoes on Russia Kamchatka Peninsula

Experiments

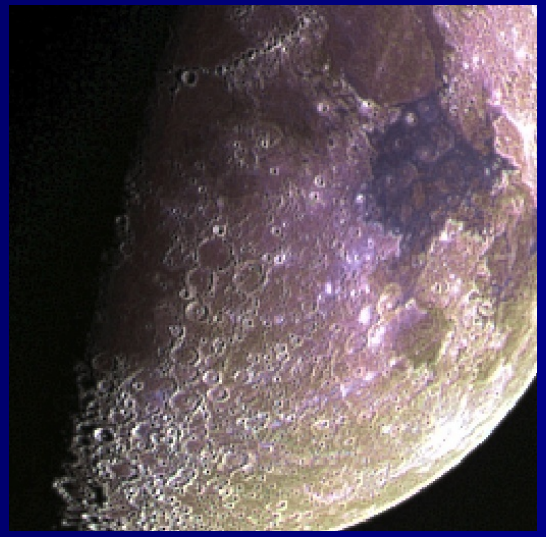

Moon

http://bf-astro.com/

Orion Nebula

How to Choose Fractional Order?

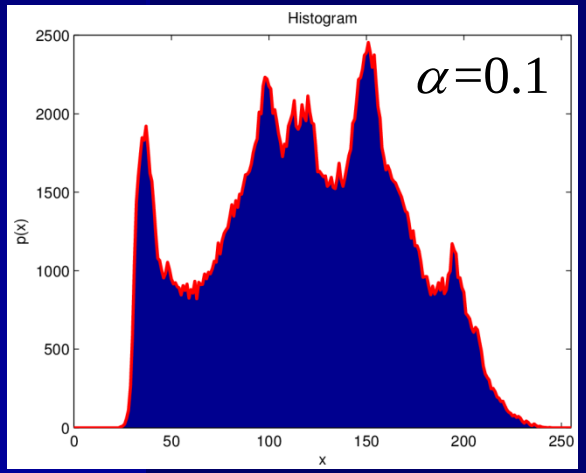

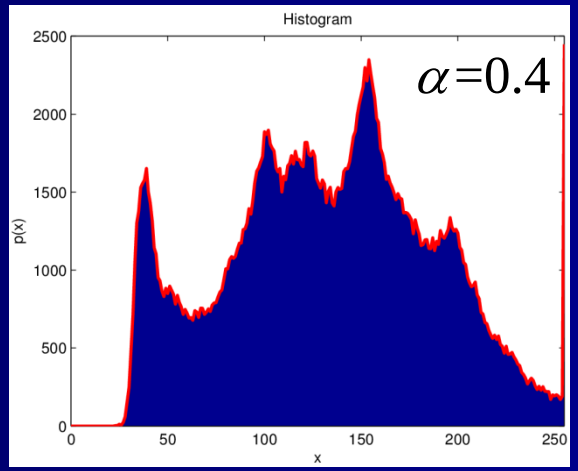

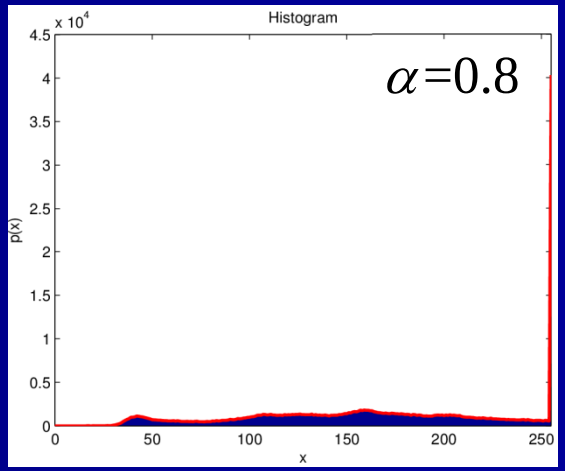

Unsupervised optimization algorithm

Let: $\Omega^{(\alpha)} := \{(x,y)|G^{(\alpha)}(x,y) = L\}$

$N^{(\alpha)}$ is the size of $\Omega^{(\alpha)}$

- $N^{(\alpha)}$ increases when α increases.
- Image is under-enhanced when $N^{(\alpha)}$ is small.
- Image is over-enhanced when $N^{(\alpha)}$ is large.

$$\widehat{\alpha} = \arg\min_{\alpha} J(\alpha) \quad (4)$$

$$M(x) = \begin{cases} (\frac{x}{5})^2, & x \in [0, 25) \\ 50 - (\frac{x-50}{5})^2, & x \in [25, 150) \\ 50, & x \in [50, 150), \\ \frac{250-x}{2}, & x \in [150, 250) \\ 0, & x \in [250, 255] \end{cases}$$

$$J(\alpha) = \sum_{(x,y)\in\Omega^{(\alpha)}} |G^{(\alpha)}(x,y) - G(x,y) - M(avg)|/N^{(\alpha)}$$

Experiments

$\alpha = 0.32$

$\alpha = 0.28$

Conclusion

- The digital fractional order Savitzky-Golay differentiator is proposed, see [2];
- The fractional order image enhancing method is proposed, see [3];
- An unsupervised optimization algorithm is proposed for choosing the fractional order, see [3];

Fractional Order Image Edge Detection

- First-Order Edge Detector: Roberts, Prewitt and Sobel[1]
  - high false reject rate (FRR)
- Second-Order Edge Detector: Laplacian of Gaussian[1]
  - high false accept rate (FAR)
- Fractional-Order Edge Detector[4]
  - high density noise

Motivation

- Fractional differential-based approach
- Robust image edge detection
- Accurate
- Immunity to noise

Outlines

- Implementation
- Analysis
  - Frequency-domain analysis
  - Parameter analysis
- Experiments
  - Evaluation method
  - Comparison analysis
  - Robustness analysis

Implementation

Fractional differential mask for edge detection

- Riemann-Liouville fractional integral[5]:

$$ {}_aI_t^{\alpha} f(t) = \frac{1}{\Gamma(\alpha)} \int_a^t (t-\tau)^{\alpha-1} f(\tau) d\tau, \qquad t \in [a, b] $$

- Rewrite (1) by convolution formula,

$$ {}_aI_t^{1-\alpha} f(t) = \frac{t^{-\alpha} * f(t)}{\Gamma(1-\alpha)} = h(t, \alpha) * f(t) \qquad (5) $$

Implementation

Fractional differential mask for edge detection

- Riemann-Liouville fractional derivative:

$$ {}_aD_t^{\alpha} f(t) = \frac{d}{dt}\, {}_aI_t^{1-\alpha} f(t) = \frac{d}{dt}\Big(h(t,\alpha) * f(t) \Big) \tag{6} $$

$$ = h'(t,\alpha) * f(t). $$

$$ h(t,\alpha) = \frac{t^{-\alpha}}{\Gamma(1-\alpha)} \tag{7} $$

- Expand to 2-D:

$$ t \to \sqrt{x^2 + y^2} \tag{8} $$

$$ h(x,y,\alpha) = \frac{(x^2+y^2)^{-\alpha/2}}{\Gamma(1-\alpha)} \tag{9} $$

Implementation

Fractional differential mask for edge detection

- 2-D formulas:

$$
\begin{aligned}
{}_aD_x^{\alpha} f(x,y) &= \frac{\partial h(x,y,\alpha)}{\partial x} * f(x,y) \\
&= H_x(x,y,\alpha) * f(x,y),
\end{aligned}
\tag{10}
$$

Fractional-order differential mask (FDM)

$$
\begin{aligned}
{}_aD_y^{\alpha} f(x,y) &= \frac{\partial h(x,y,\alpha)}{\partial y} * f(x,y) \\
&= H_y(x,y,\alpha) * f(x,y).
\end{aligned}
\tag{11}
$$

Implementation

Fractional differential mask for edge detection

- FDM equations:

$$H_x(x,y,\alpha) = -\frac{\alpha}{\Gamma(1-\alpha)} x \left(x^2+y^2\right)^{-\alpha/2-1}; \quad (12)$$

$$H_y(x,y,\alpha) = -\frac{\alpha}{\Gamma(1-\alpha)} y \left(x^2+y^2\right)^{-\alpha/2-1}. \quad (13)$$

Implementation

Fractional differential mask for edge detection

- Discrete FDM equations:

$$H_x(x_M, y_N, \alpha) = -\frac{\alpha x_M}{\Gamma(1-\alpha)}\left(x_M^2 + y_N^2\right)^{-\alpha/2-1}; \qquad (14)$$

$$H_y(x_M, y_N, \alpha) = -\frac{\alpha y_N}{\Gamma(1-\alpha)}\left(x_M^2 + y_N^2\right)^{-\alpha/2-1}. \qquad (15)$$

Here $x_M = -M, -M+1, \ldots M$ $\quad y_N = -N, -N+1, ; .. N$

$H_x(0,0,\alpha) = 0$,and $H_y(0,0,\alpha) = 0$

Implementation

Fractional differential mask for edge detection

- When $\alpha = 0.5$, 5×5 FDM:

$$\begin{pmatrix} 0.0419 & 0.0377 & 0 & -0.0377 & -0.0419 \\ 0.0755 & 0.1186 & 0 & -0.1186 & -0.0755 \\ 0.0997 & 0.2821 & 0 & -0.2821 & -0.0997 \\ 0.0755 & 0.1186 & 0 & -0.1186 & -0.0755 \\ 0.0419 & 0.0377 & 0 & -0.0377 & -0.0419 \end{pmatrix}$$

$$\begin{pmatrix} 0.0419 & 0.0755 & 0.0997 & 0.0755 & 0.0419 \\ 0.0377 & 0.1186 & 0.2821 & 0.1186 & 0.0377 \\ 0 & 0 & 0 & 0 & 0 \\ -0.0377 & -0.1186 & -0.2821 & -0.1186 & -0.0377 \\ -0.0419 & -0.0755 & -0.0997 & -0.0755 & -0.0419 \end{pmatrix}.$$

Implementation

Image edge detection algorithm flow

- Step 1: Calculate:

$$M(x,y) = \sqrt{(D_x^\alpha f(x,y))^2 + (D_y^\alpha f(x,y))^2}$$

$$\varphi(x,y) = \tan^{-1}(D_y^\alpha f(x,y) / D_x^\alpha f(x,y))$$

- Step2: Find an edge direction.
- Step3: Non-maximum suppression.
- Step4: Hysteresis Thresholding.
- Step5: Link edge.

Implementation

Image edge detection algorithm flow

```
function eout=ch_fedge(a,alpha,width)
if ~isa(a,'double') && ~isa(a,'single'), a = im2single(a);end
[m,n] = size(a);e = false(m,n);PercentOfPixelsNotEdges = .7;
ThresholdRatio = .4;chw=-alpha/gamma(1-alpha);
[x,y]=meshgrid(-width:width,-width:width);
dgau2D=x.*(x.*x+y.*y).^(-alpha/2-1)*chw;
dgau2D(width+1,width+1)=0;
ax = imfilter(a, dgau2D, 'conv','replicate');
ay = imfilter(a, dgau2D', 'conv','replicate');
mag = sqrt((ax.*ax) + (ay.*ay));magmax = max(mag(:));
if magmax>0,mag = mag / magmax;end  counts=imhist(mag, 64);
highThresh = find(cumsum(counts) > ...
PercentOfPixelsNotEdges*m*n,1,'first') / 64;
lowThresh = ThresholdRatio*highThresh;
thresh = [lowThresh highThresh];idxStrong = [];
```

Implementation

Image edge detection algorithm flow

```
for dir = 1:4
    idxLocalMax = cannyFindLocalMaxima(dir,ax,ay,mag);
    idxWeak = idxLocalMax(mag(idxLocalMax) > lowThresh);
    e(idxWeak)=1;
    idxStrong = [idxStrong;...
                 idxWeak(mag(idxWeak) > highThresh)];
end
if ~isempty(idxStrong)
    rstrong = rem(idxStrong-1, m)+1;
    cstrong = floor((idxStrong-1)/m)+1;
    e = bwselect(e, cstrong, rstrong, 8);
    e = bwmorph(e, 'thin', 1);
end
eout = e;
```

Analysis

Parameter analysis

- $M = 5$
- $\alpha : 0 \longrightarrow 1$

Original image

- Smoothing ↘
- Enhancing ↗

Analysis

Parameter analysis

- $\alpha = 0.9$
- $M : 2 \longrightarrow 40$

- Smoothing ↗
- Enhancing ↘

Analysis

Parameter and noise immunity

- $M = 4$
- $\alpha : 1 \longrightarrow 0$

Noisy image: Gaussian noise with zero-mean and variance $\sigma^2 = 0.01$

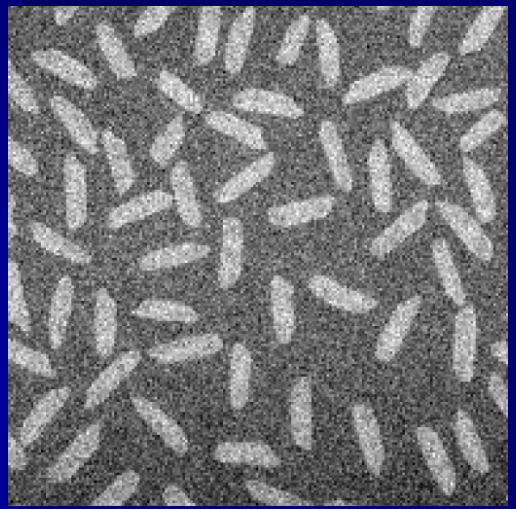

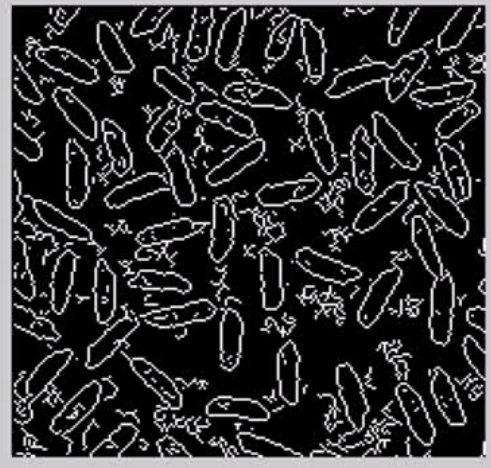

- Noise immunity ↗
- Enhancing ↘

Analysis

Parameter and noise immunity

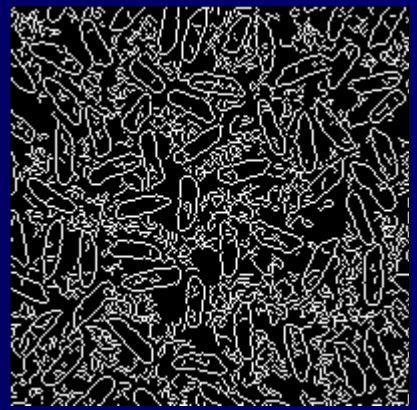

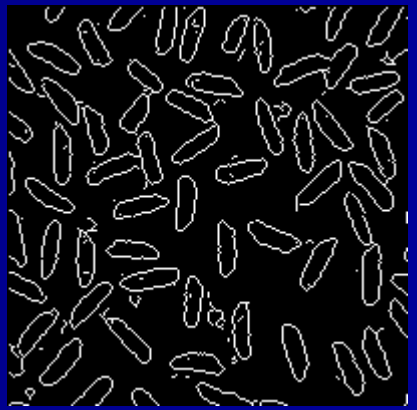

$M = 2$ $M = 3$ $M = 4$

- $\alpha = 0.5$
- Noise immunity ↗
- Enhancing ↘

Analysis

Conclusion

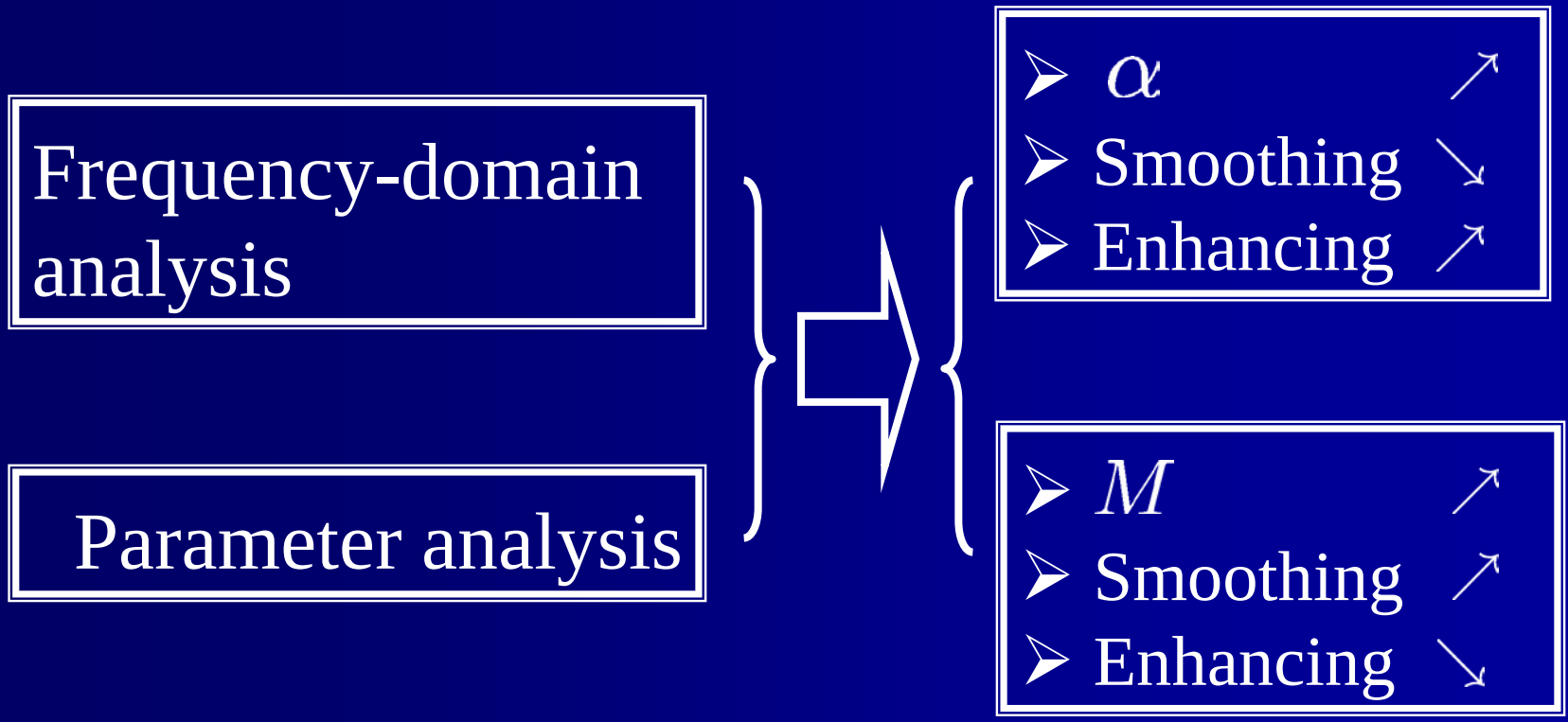

Experiments

Evaluation method

- False Reject Rate (FRR):

$$\mu_{FRR} = \frac{\Psi(A - A \bigcap B)}{\Psi(A)}$$

- False Accept Rate (FAR):

$$\mu_{FAR} = \frac{\Psi(\overline{A} \bigcap B)}{\Psi(B)}$$

- Single-Pixel-Detecting (SPD):

$$\mu_{SPD} = \frac{\Psi(\varphi(B))}{\Psi(B)}$$

✓ $\Psi(X)$ denotes the number of elements in X

✓ μ_{FRR} ↘ μ_{FAR} ↘ accuracy ↗

✓ φ is the typical thinning operator [6]

✓ Single edge: $\mu_{SPD} = 1$

Experiments: *Comparison analysis*

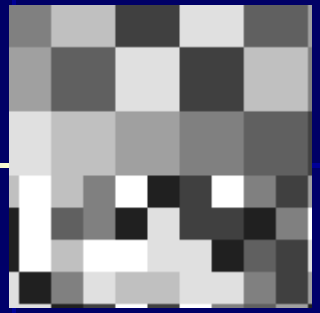

(a)Multi-scale linear edge image

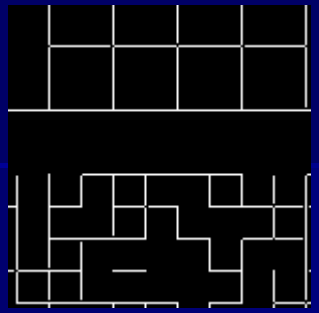

(b) Robert edge detector

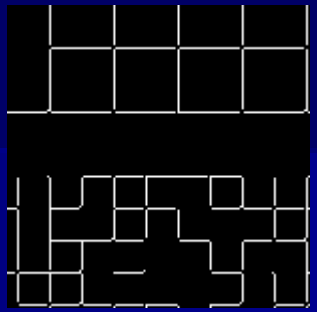

(c) Prewitt edge detector

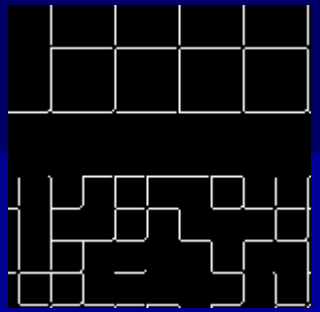

(d) Sobel edge detector

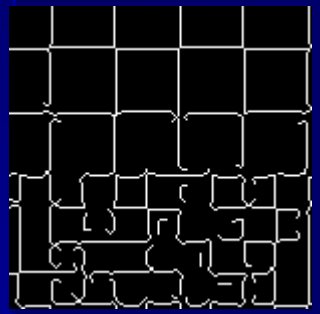

(e) LoG edge detector

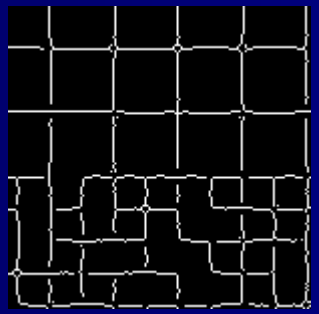

(f) Canny edge detector

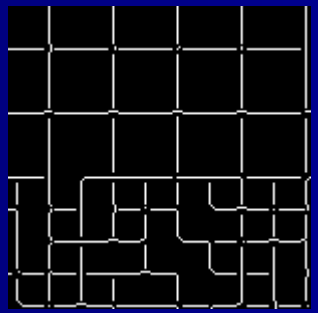

(g) Oustaloup edge detector

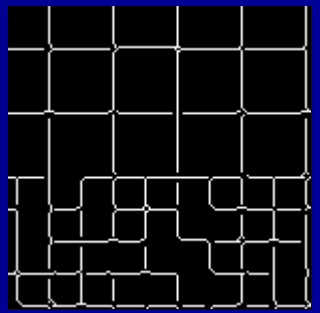

(h) Proposed edge detector

Conclusion: 1.Better than the Roberts, Prewitt,Sobel, LoG and Canny edge detectors;
2.Similar with the Oustaloup edge detector.

Experiments: *Comparison analysis*

(a)Nonlinear edge image

(b) Robert edge detector

(c) Prewitt edge detector

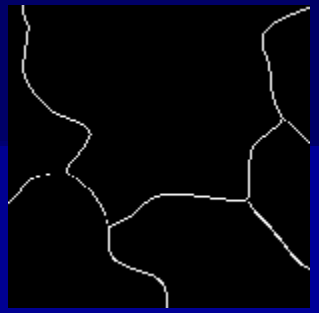

(d) Sobel edge detector

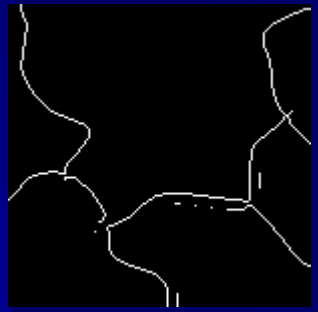

(e) LoG edge detector

(f) Canny edge detector

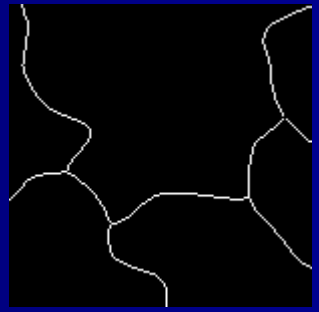

(g) Oustaloup edge detector

(h) Proposed edge detector

Conclusion: 1.Better than the Roberts, Prewitt,Sobel and LoG edge detectors;
2.Similar with the Canny and Oustaloup edge detector.

Experiments: *Comparison analysis*

Table 1: Quantitative comparison among the proposed method and six typical methods

	Linear		Nonlinear	
Method	μ_{FR}	μ_{SPD}	μ_{FR}	μ_{SPD}
Roberts	0.0852(4)	0.9844(6)	0.1246(7)	0.8214(7)
Prewitt	0.0887(6)	0.9892(3)	0.0622(5)	0.9966(4)
Sobel	0.0882(5)	0.9887(4)	0.0416(4)	0.9788(6)
LoG	0.1348(7)	0.9850(5)	0.1041(6)	0.9956(5)
Canny	0.0226(3)	0.9949(2)	0.0052(3)	**0.9995**(1)
Oustaloup	0.0173(2)	**0.9991**(1)	0.0034(2)	0.9986(3)
Proposed	**0.0135**(1)	0.9952(2)	**0.0033**(1)	0.9988(2)

$\mu_{FR} = \mu_{FRR} + \mu_{FAR}$

Experiments

Robustness analysis

- X Axis
  - ✓ Noisy image
  - ✓Signal To Noise Rate (SNR)
- Y Axis
  - ✓ False rate (FR)
- Red curve
- Better than the other detectors

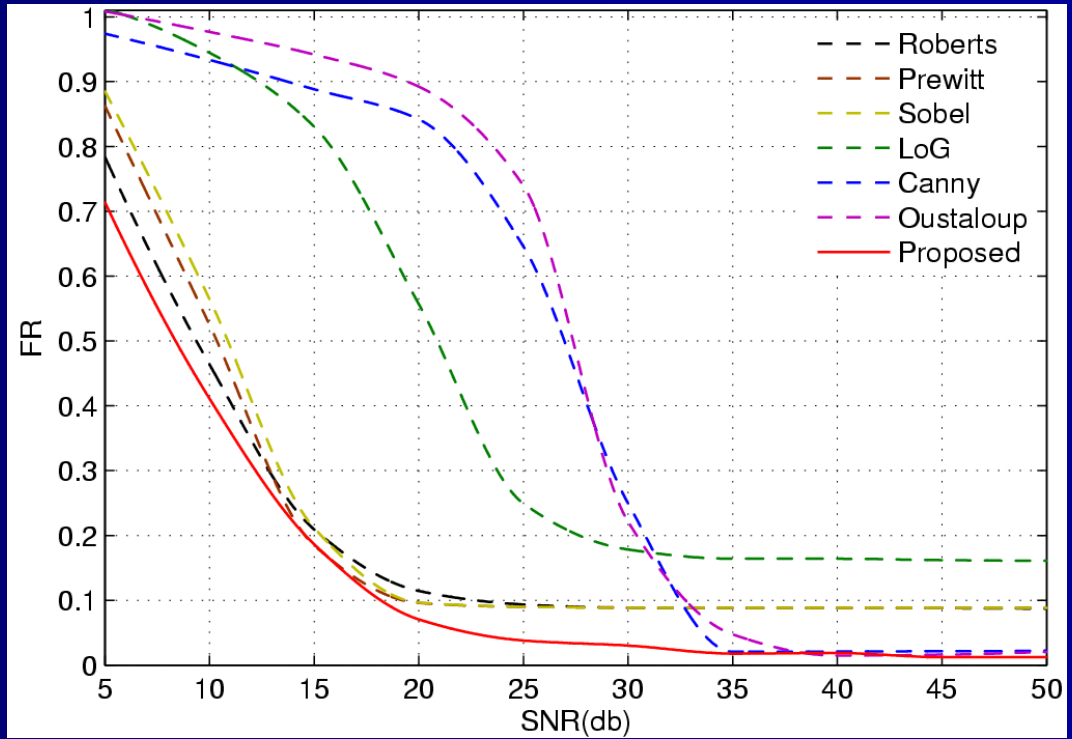

Fig. FR comparison among the seven edge detectors for the multi-scale linear edge noisy images with different SNRs

Experiments

Robustness analysis

- X Axis
  - ✓ Noisy image
  - ✓Signal To Noise Rate (SNR)
- Y Axis
  - ✓ False rate (FR)

- Robustness is better.

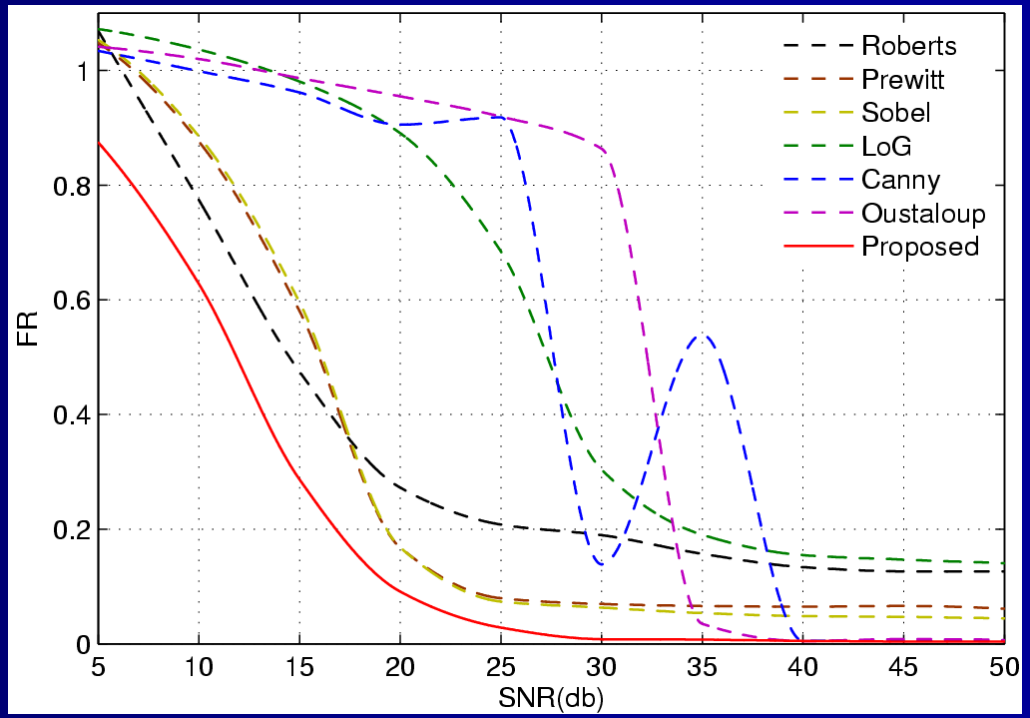

Fig. FR comparison among the seven edge detectors for the nonlinear edge noisy images with different SNRs

Conclusion

- A new fractional differential-based method is proposed for robust image edge detection, see [6];
- Frequency domain analysis;
- Good edge-detecting capability and robustness;
- Fast, real-time systems.

Fractional Order Image Denoising

Problem Description

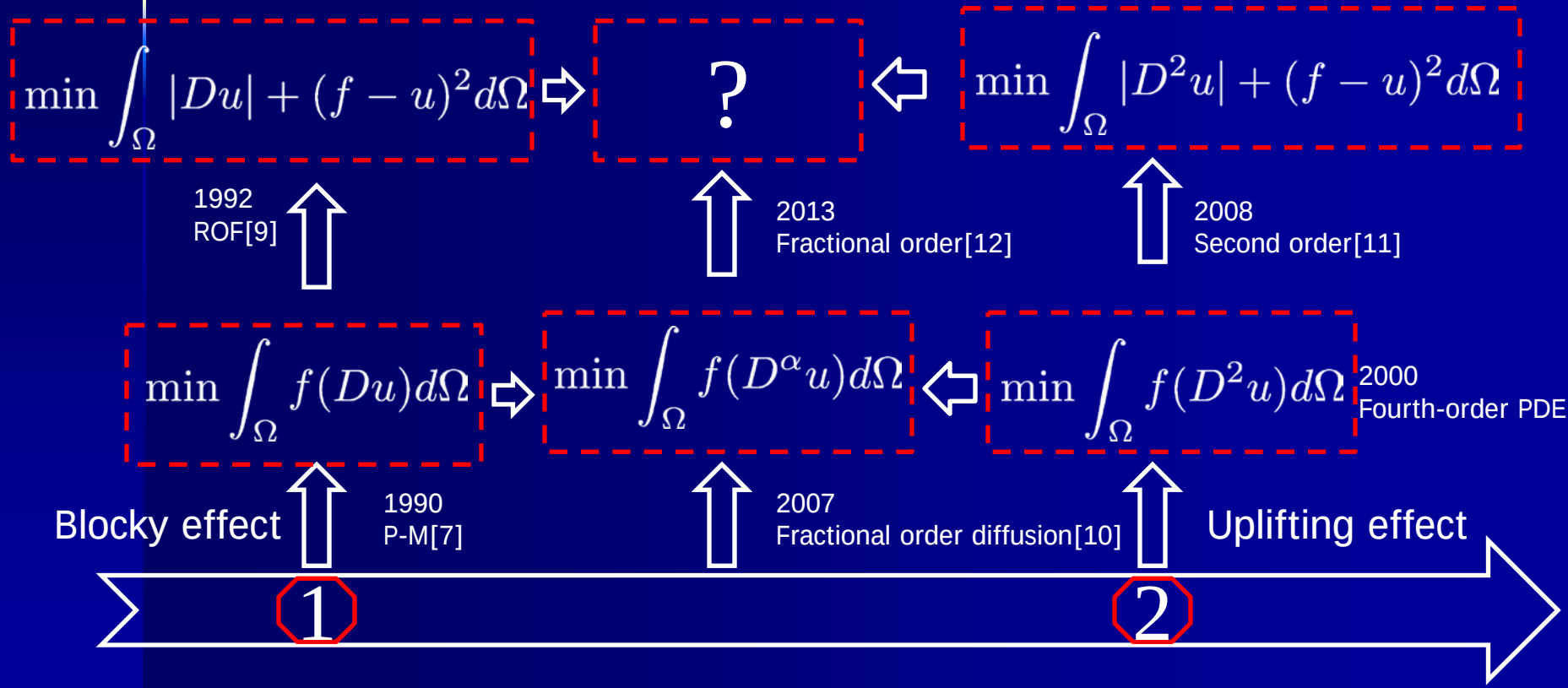

Outline

- Majorization-Minimization (MM) Method
- Fractional Order Total Variation(TV)-L2 Model
- Majorization of $\mathrm{TV}_p^{\alpha}(u)$
- Numerical Scheme
- Experiments

Why MM Method ?

- Continuous Domain[13-16]:
  - Newton's Method
  - Duality Theory
  - Euler-Lagrange Equation
  - FTVd Method
- Discrete Domain[17-18]
  - Majorization-Minimization (MM) Method

Majorization-Minimization (MM) Method

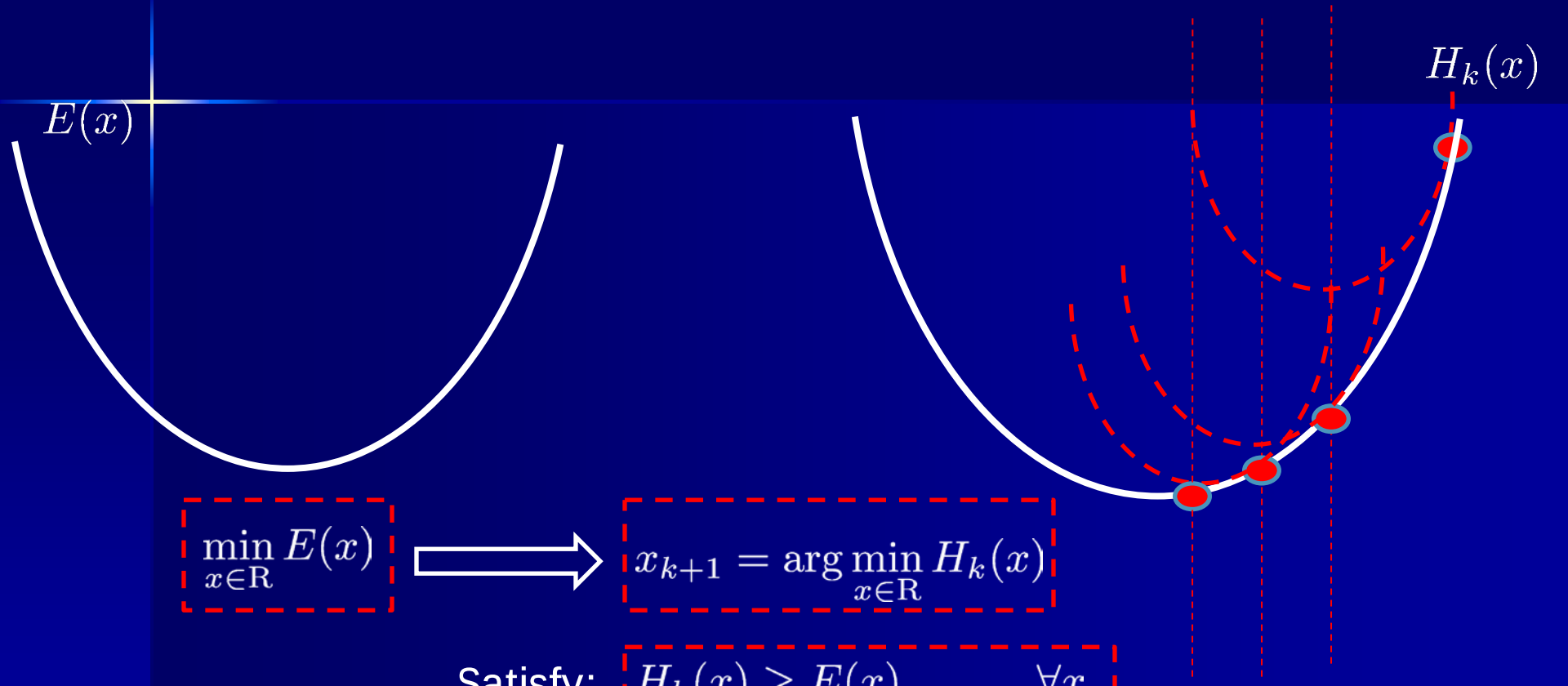

$$\min_{x \in \mathrm{R}} E(x)$$

$$x_{k+1} = \arg\min_{x \in \mathrm{R}} H_k(x)$$

Satisfy:

$$H_k(x) \geq E(x), \qquad \forall x$$

$$H_k(x_k) = E(x_k)$$

Fractional Order TV-L2 Model

$$\widehat{u} = \arg\min_{u} \left\{ E(u) = \|f - u\|_2^2 + \lambda \mathrm{TV}_p^{\alpha}(u) \right\} \tag{16}$$

Data term Regularization term

$$\mathrm{TV}_p^{\alpha}(u) = \sum_{n \in \Omega} \|D^{\alpha} u(n)\|_p$$

$$\|\mathrm{D}^{\alpha} u(n)\|_1 = |\mathrm{D}_h^{\alpha} u(n)| + |\mathrm{D}_v^{\alpha} u(n)|$$

$$\|\mathrm{D}^{\alpha} u(n)\|_2 = \sqrt{(\mathrm{D}_h^{\alpha} u(n))^2 + (\mathrm{D}_v^{\alpha} u(n))^2}$$

λ: regularization parameter;

D_h^{α}: horizontal fractional order derivative ;

D_v^{α} : vertical fractional order derivative ;

f: Noisy image;
u: Clean image;

$\|u\|_{\nu}$: ν-norm;

Majorization of $\mathrm{TV}_p^\alpha(u)$

Assume

$$Q_{(k,1)}(u) = \tfrac{1}{2}\mathrm{TV}_1^\alpha(u_k) + \tfrac{1}{2}u^T(\mathrm{D}^\alpha)^T V_{(k,1)}^{-1}\mathrm{D}^\alpha u = \mathrm{C}_1^\alpha(u_k) + \tfrac{1}{2}u^T(\mathrm{D}^\alpha)^T V_{(k,1)}^{-1}\mathrm{D}^\alpha u,$$

$$\mathrm{D}^\alpha = [(\mathrm{D}_h^\alpha)^T, (\mathrm{D}_v^\alpha)^T]^T$$

$$V_{(k,1)} = \mathrm{diag}(\Lambda_k^h, \Lambda_k^v)$$

$$\Lambda_k^v = \mathrm{diag}(|\mathrm{D}_v^\alpha u_k|)$$

$$\Lambda_k^h = \mathrm{diag}(|\mathrm{D}_h^\alpha u_k|)$$

$$Q_{(k,1)}(u) \geq \mathrm{TV}_1^\alpha(u) \qquad Q_{(k,1)}(u_k) = \mathrm{TV}_1^\alpha(u_k)$$

$Q_{(k,1)}(u)$ is the majorization of $\mathrm{TV}_1^\alpha(u)$

Majorization of $\mathrm{TV}_p^\alpha(u)$

Assume

$$Q_{(k,2)}(u) = \mathrm{TV}_2^\alpha(u_k) + \tfrac{1}{2}u^T(\mathrm{D}^\alpha)^T V_{(k,2)}^{-1}\mathrm{D}^\alpha u = \mathrm{C}_2^\alpha(u_k) + \tfrac{1}{2}u^T(\mathrm{D}^\alpha)^T V_{(k,2)}^{-1}\mathrm{D}^\alpha u,$$

$$V_{(k,2)} = \mathrm{diag}(v_k, v_k)$$

$$v_k = \mathrm{diag}(\sqrt{(\mathrm{D}_h^\alpha u_k)^2 + (\mathrm{D}_v^\alpha u_k)^2})$$

$$Q_{(k,2)}(u) \geq \mathrm{TV}_2^\alpha(u)$$

$$Q_{(k,2)}(u_k) = \mathrm{TV}_2^\alpha(u_k)$$

$Q_{(k,2)}(u)$ is the majorization of $\mathrm{TV}_2^\alpha(u)$

Majorization of $\mathrm{TV}_p^\alpha(u)$

The majorization of $\mathrm{TV}_p^\alpha(u)$ is

$$Q_{(k,p)}(u) = \mathrm{C}_p^\alpha(u_k) + \tfrac{1}{2}u^T(\mathrm{D}^\alpha)^T V_{(k,p)}^{-1}\mathrm{D}^\alpha u.$$

So, the majorization of the fractional order TV model is

$$H_{(k,p)}(u) = \|f-u\|_2^2 + \tfrac{1}{2}u^T(\mathrm{D}^\alpha)^T V_{(k,p)}^{-1}\mathrm{D}^\alpha u + \mathrm{C}_p^\alpha(u_k).$$

constant

Thus, the *u* can be estimated by solving a sequence of optimization problems

$$u_{k+1} = \arg\min_u \left\{\|f-u\|_2^2 + \tfrac{\lambda}{2}u^T(\mathrm{D}^\alpha)^T V_{(k,p)}^{-1}\mathrm{D}^\alpha u\right\}.$$

It leads to a linear system: $\left(I + \lambda(\mathrm{D}^\alpha)^T V_{(k,p)}^{-1}\mathrm{D}^\alpha\right)u_{k+1} = f,$

Numerical Scheme

1. Let the input image be f and set $k = 0$ and $u_k = f$. Initialize $K_{\sigma'}$, σ, M, N and iteration number K_{iter}.
2. Set $u_k = K_{\sigma'} * u_k$ and $\lambda_k^p = MN\sigma^2 / 2\mathrm{TV}_p^\alpha(u_k)$.
3. Compute $A_k = \left(I + \lambda_k^p (\mathrm{D}^\alpha)^T V_{(k,p)}^{-1} \mathrm{D}^\alpha\right)$.
4. Compute u_{k+1} by using the conjugate gradient algorithm to solve the linear system $A_k u_{k+1} = f$.
5. If $k = K_{iter}$, stop; else, set $k = k + 1$ and go to step 2.

Experiments: *Restraint of block effect*

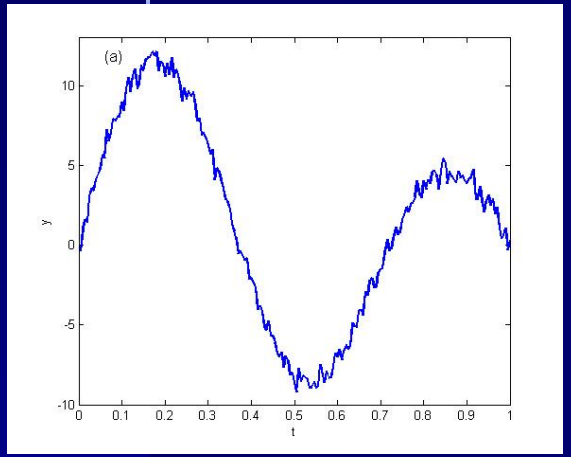

Noisy signal

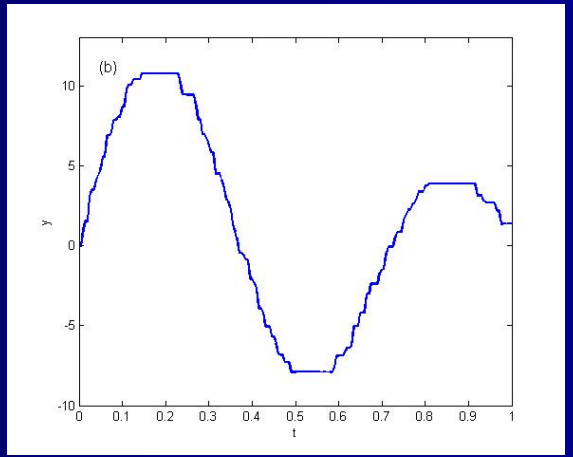

TV-L2 model

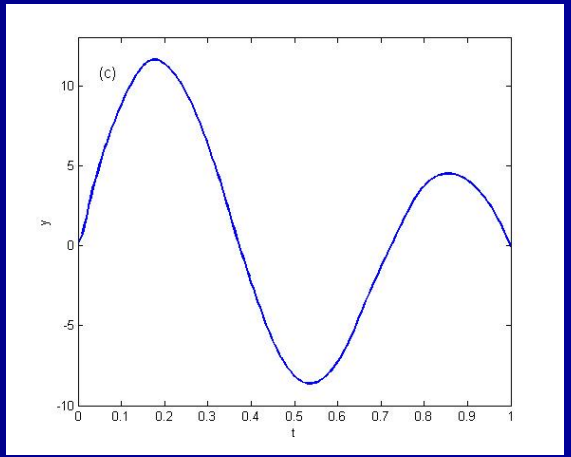

Fractional order TV-L2 model

Conclusion: the proposed fractional order TV-L2 model can reduce blocky effect.

Experiments: *Analysis of denoising performance*

PSNR: peak signal to noise ratio

Table 1: PSNR quantitative comparison among five denoising models

Image	SD	IP-M	F-O-PDE	IF-O-PDE	ROF	TV_2^{α}-L^2
Barbara	10	31.2427	29.3776	29.3777	31.0871	**31.3792**
	20	26.6231	24.8155	24.8156	26.8212	**26.9798**
	30	24.4496	22.9267	22.9273	24.7415	**24.8166**
Lena	10	33.6393	31.5440	31.5442	33.8378	**34.7437**
	20	29.7665	27.8080	27.8098	30.4101	**31.4387**
	30	27.4437	26.0883	26.1019	28.5889	**29.6095**
Peppers	10	33.6967	31.8199	31.8205	33.8715	**33.9328**
	20	30.0275	28.0437	28.0457	30.1768	**30.4965**
	30	27.4982	26.1613	26.1694	28.2689	**28.8305**

IP-M: Improved Perona and Malik model [7]; F-O-PDE: fourth order PDE model [8]; IF-O-PDE: improved fourth order PDE model[19]; ROF model [9]; proposed fractional order TV2-L2 model.

Conclusion: the denoising performance proposed fractional order TV_2-L2 model is better than the other four methods.

Experiments: *Analysis of denoising performance*

Table 1: PSNR quantitative comparison between TV_1^{α}-L^2 and TV_2^{α}-L^2 model

	Barbara			Lena			Peppers			Goldhill		
Model	10	20	30	10	20	30	10	20	30	10	20	30
$TV_2^{1.6}$-L^2	31.4118	26.8263	24.5162	34.4373	31.1986	29.5400	33.8179	30.1648	28.8539	32.1030	28.8404	27.7313
$TV_1^{1.6}$-L^2	31.4057	26.7565	23.8417	32.6776	27.1440	25.0362	32.4445	26.9766	24.2010	31.7602	26.8850	25.3306

Conclusion: the denoising performance proposed fractional order TV_2-L2 model is better than fractional order TV_1-L2 model.

Experiments: *Analysis of denoising performance*

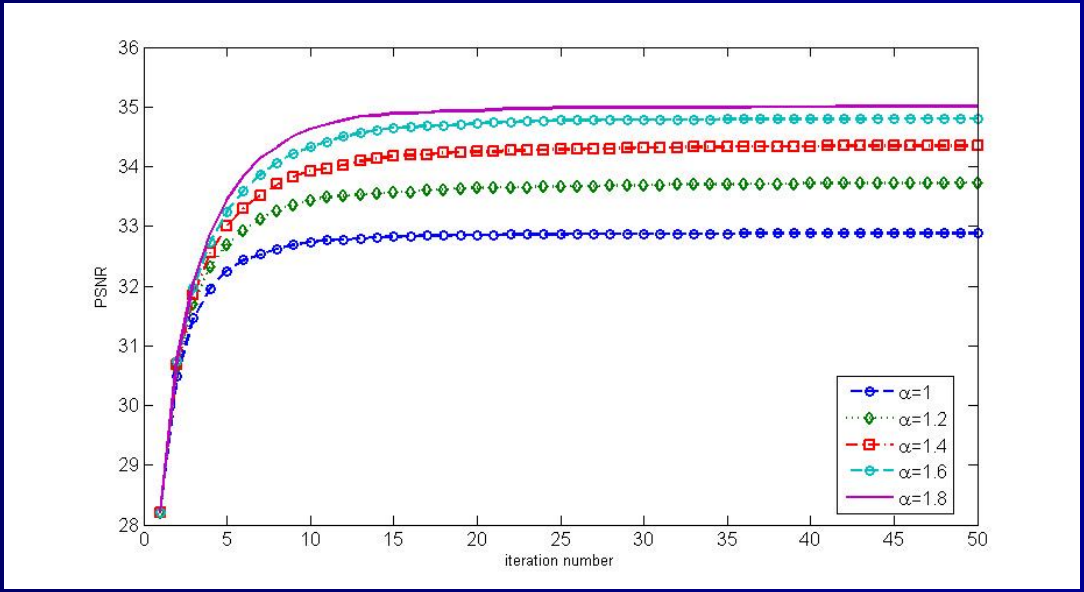

Relation between the iteration number and PSNR value

Conclusion: the method is stable after 15 iterations.

Experiments:

Lung nodule segmentation experiment

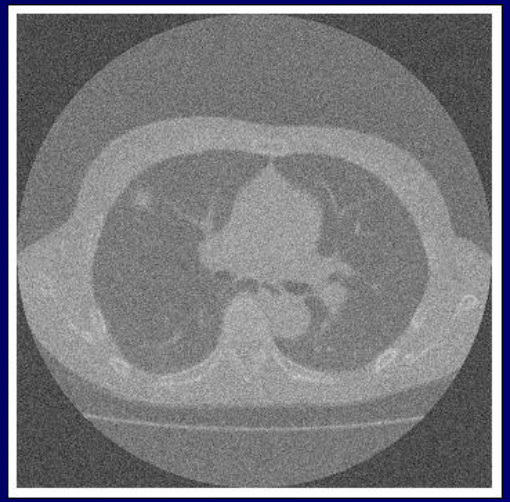

Noisy lung nodule CT image

Partial enlarged view of the segmented result

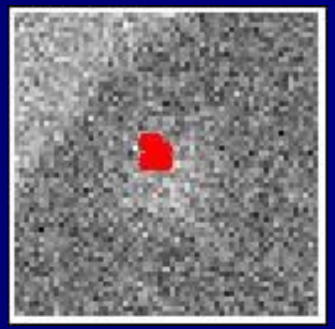

$\mathrm{TV}_2^1 - L^2$

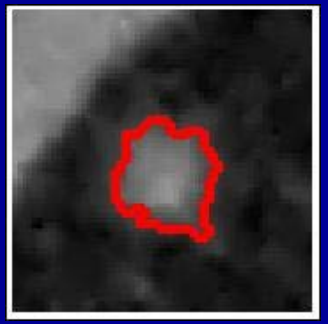

$\mathrm{TV}_2^{1.5} - L^2$

Conclusion: 1.fractional order TV-L2 denoising method is helpful for improving the accuracy of the post-processing technologies in the lung nodule CT image segmentation. 2. the detected edge of $\mathrm{TV}_2^{1.5} - L^2$ is more accurate than that of $\mathrm{TV}_2^1 - L^2$

Experiments:

Cardiac muscular segmentation experiment

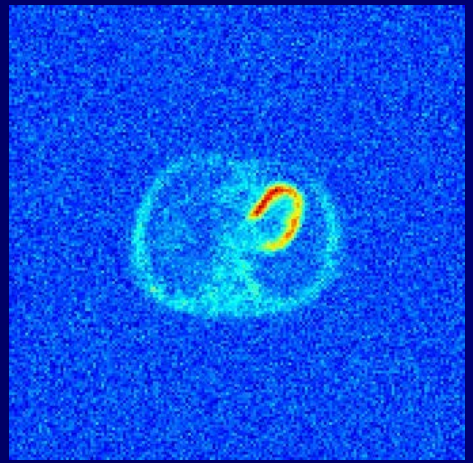

Noisy cardiac muscular PET image

Partial enlarged view of the segmented result

$\mathrm{TV}_2^1 - L^2$

$\mathrm{TV}_2^{1.5} - L^2$

Conclusion: 1. fractional order TV-L2 denoising method is helpful for improving the accuracy of the post-processing technologies in the cardiac muscular PET image segmentation. 2. the detected edge of $\mathrm{TV}_2^{1.5} - L^2$ is more accurate than that of $\mathrm{TV}_2^1 - L^2$

Conclusion

- Two fractional order TV-L2 models are constructed, see [12];
- Majorization-minimization algorithm was used to solve fractional TV optimization problem, see [12];
- Majorizors of two fractional order TV regularizers are obtained in one uniform formula, see [12];
- Avoid the blocky effect.

Fractional Order Level Set Model

Introduction

What is the Level Set Method?

LSM is a numerical technique for tracking interfaces and shapes.

What is Level Set Good for? [20-27]

- Image Segmentation
- Tracking
- Computer Graphics
- Computational Geometry
- Computational fluid dynamics

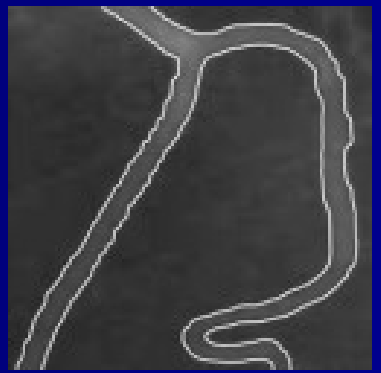

Fractional Order Level Set Model

Problem Description

$$\min \int_{\Omega} (\lambda_1 |I - c_1|^2 H(\phi) + \lambda_2 |I - c_2|^2 (1 - H(\phi)) + \mu \delta(\phi) |D^{\alpha} \phi|) d\Omega$$

$$\min \int_{\Omega} (\lambda_1 |I - c_1|^2 H(\phi) + \lambda_2 |I - c_2|^2 (1 - H(\phi)) + \mu \delta(\phi) |D \phi|) d\Omega$$

C-V Model [20] 2001

$$\begin{aligned} \min E(f_1(x), f_2(x), \phi) &= \lambda_1 \int (\int_{\Omega} K_{\sigma}(x-y) |I(y) - f_1(x)|^2 H(\phi(y)) dy) dx \\ &+ \lambda_2 \int (\int_{\Omega} K_{\sigma}(x-y) |I(y) - f_1(x)|^2 (1 - H(\phi(y))) dy) dx \\ &+ \mu \int_{\Omega} \delta(\phi) |D^{\alpha} \phi| d\Omega \end{aligned}$$

$$\begin{aligned} \min E(f_1(x), f_2(x), \phi) &= \lambda_1 \int (\int_{\Omega} K_{\sigma}(x-y) |I(y) - f_1(x)|^2 H(\phi(y)) dy) dx \\ &+ \lambda_2 \int (\int_{\Omega} K_{\sigma}(x-y) |I(y) - f_1(x)|^2 (1 - H(\phi(y))) dy) dx \\ &+ \mu \int_{\Omega} \delta(\phi) |D \phi| d\Omega \end{aligned}$$

RSF Model [21] 2008

Outline

- C-V Model
- Fractional Order C-V Model
- RSF (Region-Scalable Fitting) Model
- Fractional Order RSF Model
- Numerical Algorithm
- Experiments

C-V Model [20]

Model description:

$$\min \int_{\Omega} (\lambda_1 |I - c_1|^2 H(\phi) + \lambda_2 |I - c_2|^2 (1 - H(\phi)) + \mu \delta(\phi) |D\phi|) d\Omega$$

$$c_1(\phi) = \frac{\int_{\Omega} I(x,y) H(\phi(x,y)) dxdy}{\int_{\Omega} H(\phi(x,y)) dxdy} \quad (17) \quad H(\phi) = \begin{cases} 1, & \phi \geq 0 \\ 0, & \phi < 0 \end{cases}$$

$$c_2(\phi) = \frac{\int_{\Omega} I(x,y)(1 - H(\phi(x,y))) dxdy}{\int_{\Omega} (1 - H(\phi(x,y))) dxdy} \quad (18)$$

λ_1 and λ_2 are positive constants

将 $E(C)$ 改成 $E(\phi)$

C-V Model

$$\phi(x,y,t) = \begin{cases} D(x,y,t), & (x,y) \in \Omega_1 \\ 0, & (x,y) \in C \\ -D(x,y,t), & (x,y) \in \Omega_2 \end{cases}$$

$D(x,y,t)$ is the Euclidean distance from point (x,y) to curve C at time t.

Ω_1 is inside C

Ω_2 is outside C

ϕ is the level set.

Fractional Order C-V Model

Model description:

$$\min \int_{\Omega} (\lambda_1 |I - c_1|^2 H(\phi) + \lambda_2 |I - c_2|^2 (1 - H(\phi)) + \mu \delta(\phi) |D^{\alpha} \phi|) d\Omega$$

Euler–Lagrange Equation：

$$\frac{\partial \phi}{\partial t} = \delta(\phi)[\mu div^{\alpha}(\frac{D^{\alpha \phi}}{|D^{\alpha} \phi|}) - \lambda_1 (I - c_1)^2 + \lambda_2 (I - c_2)^2] \quad (19)$$

RSF Model [21]

Model description: Region-Scalable Fitting Energy

$$\begin{aligned}\min E(f_1(x), f_2(x), \phi) &= \lambda_1 \int \left(\int_{\Omega} K_\sigma(x-y) |I(y) - f_1(x)|^2 H(\phi(y)) dy \right) dx \\ &+ \lambda_2 \int \left(\int_{\Omega} K_\sigma(x-y) |I(y) - f_1(x)|^2 (1 - H(\phi(y))) dy \right) dx \\ &+ \mu \int_{\Omega} \delta(\phi) |D\phi| d\Omega \qquad \text{Curve Length}\end{aligned}$$

$$K_\sigma(x-y) = \frac{1}{(2\pi)^{n/2}\sigma^n} \exp\left(-\frac{|x-y|^2}{2\sigma^2}\right)$$

$I(y)$ denotes the intensity of the point y in a neighborhood of x

f_1 and f_2 are two values that approximate image intensities in Ω_1 and Ω_2

Fractional Order RSF Model

Model description:

$$\begin{aligned}\min E(f_1(x), f_2(x), \phi) &= \lambda_1 \int \left(\int_{\Omega} K_\sigma(x-y) |I(y) - f_1(x)|^2 H(\phi(y)) dy \right) dx \\ &+ \lambda_2 \int \left(\int_{\Omega} K_\sigma(x-y) |I(y) - f_1(x)|^2 (1 - H(\phi(y))) dy \right) dx \\ &+ \mu \int_{\Omega} \delta(\phi) |D^\alpha \phi| d\Omega\end{aligned}$$

$$\frac{\partial \phi}{\partial t} = \delta(\phi)[\mu div^\alpha(\frac{D^{\alpha\phi}}{|D^\alpha \phi|}) - \lambda_1 e_1 + \lambda_2 e_2] \quad (20)$$

$$e_i(x) = \int K_\sigma(y-x)|I(x) - f_i(y)|^2 dy, \qquad i = 1, 2$$

Principal step of algorithm

The principal steps of the algorithm are:

1. Initialize ϕ^0 by ϕ_0, $n = 0$;
2. Fractional- Order C-V Model: Compute $c_1(\phi^n)$ and $c_2(\phi^n)$ by (17) and(18);
   Fractional- Order RSF Model: Compute $f_1(x)$,$f_2(y)$ and $K_\sigma(x-y)$;
3. Solve the Euler-Lagrange Equation in ϕ from (19) or (20), to obtain ϕ^{n+1};
4. Reinitialize ϕ locally to the signed distance function to the curve;
5. Check whether the solution is stationary. If not, $n = n + 1$ and repeat.

Intensity Homogeneity PET Cardiac Muscular Segmentation Experiment

Cardiac Muscular PET Image

Segmented Result

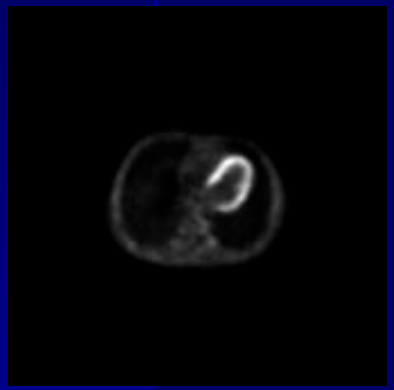

Original PET Image

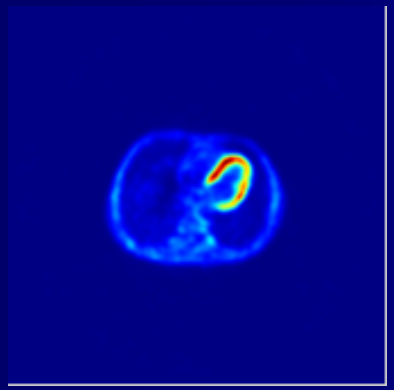

Pseudo-Color Image

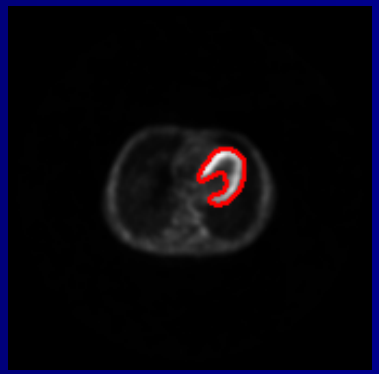

C-V Model

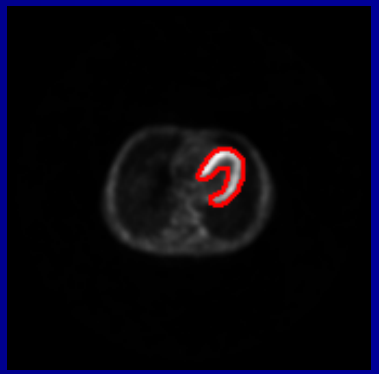

Fractional Order C-V Model $\alpha = 1.8$

Conclusion: For intensity homogeneity PET cardiac muscular image, the detected edge of fractional order CV model is more accurate than that of typical CV model.

Intensity Homogeneity PET Cardiac Muscular Segmentation Experiment

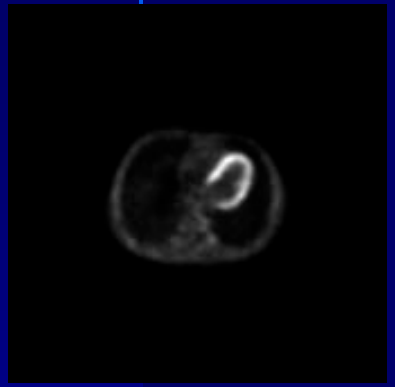

Original PET Image

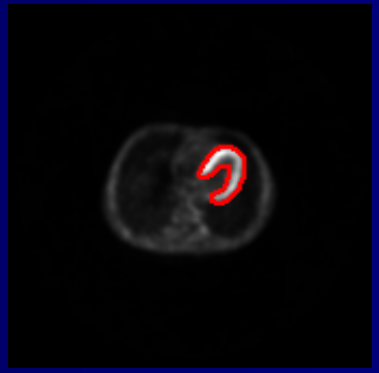

Fractional Order C-V Model

$\alpha = 1.8$

RSF Model

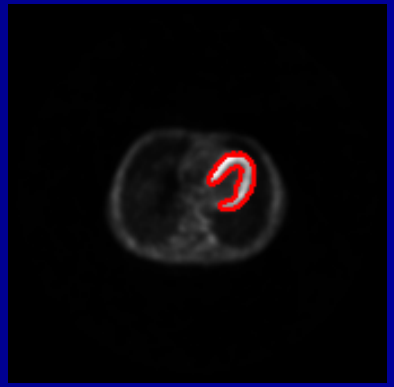

Fractional Order RSF Model

$\alpha = 1.8$

Conclusion: For intensity homogeneity PET cardiac muscular image, the detected edge of fractional order RSF model is more accurate than that of both fractional order and typical CV models.

Intensity Homogeneity PET Cardiac Muscular Segmentation Demo

Fractional Order Level Set Model

Demo: Intensity homogeneity PET cardiac muscular image

YangQuan Chen, Dingyu Xue, Dali Chen, Congrong Zhang

yangquan.chen@ucmerced.edu
yqchen@ieee.org
MESA(Mechatronics, Embedded Systems and Automation)LAB
School of Engineering, University of California, Merced, 5200 N Lake Road, Merced, CA 95343, USA

xuedingyu@ise.neu.edu.cn,
chendali@ise.neu.edu.cn
Information Science and Engineering
Northeastern University
Shenyang 110004, P R China

Intensity Inhomogeneity PET Cardiac Muscular Segmentation Experiment

Cardiac Muscular PET Image

Segmented Result

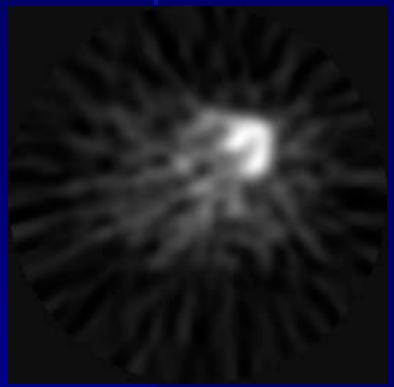

Original PET Image

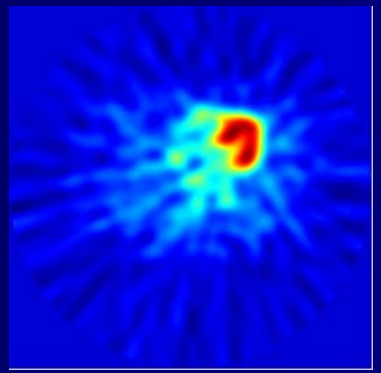

Pseudo-Color Image

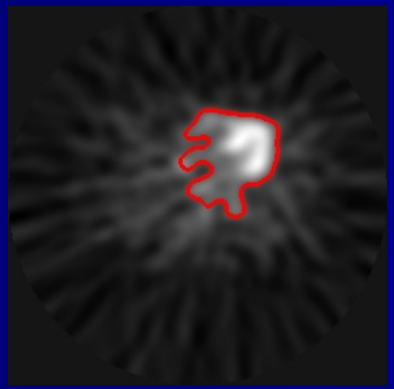

C-V Model

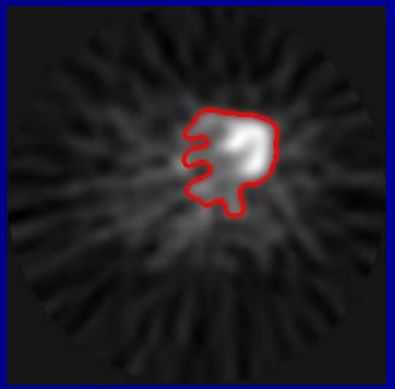

Fractional Order C-V Model $\alpha = 1.8$

Conclusion: For intensity inhomogeneity PET cardiac muscular image, both fractional order and typical CV models are not able to get satisfactory result.

Intensity Inhomogeneity PET Cardiac Muscular Segmentation Experiment

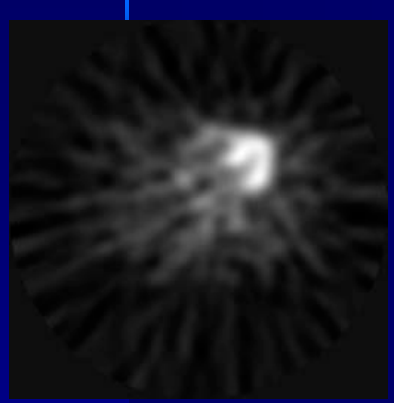

Original PET Image

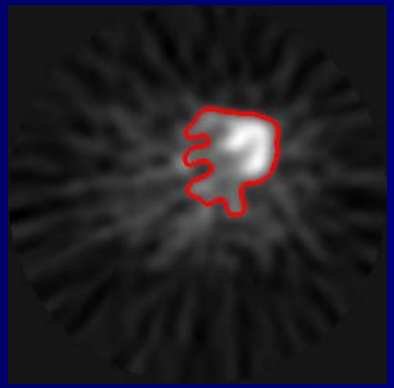

Fractional Order C-V Model

$\alpha = 1.8$

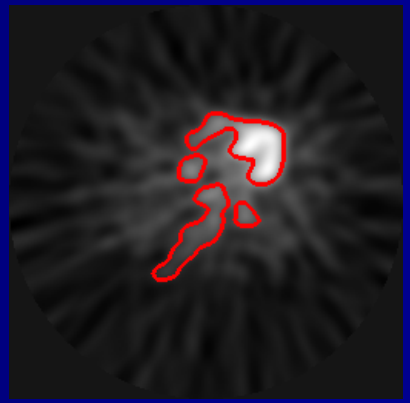

RSF Model

Fractional Order RSF Model

$\alpha = 1.8$

Conclusion: For intensity inhomogeneity PET cardiac muscular image, the detected edge of fractional order RSF model is more accurate than that of both fractional order and typical CV models.

Intensity Inhomogeneity PET Cardiac Muscular Segmentation Demo

Fractional Order Level Set Model

Demo: Intensity inhomogeneity PET cardiac muscular image

YangQuan Chen, Dingyu Xue, Dali Chen, Congrong Zhang

yangquan.chen@ucmerced.edu
yqchen@ieee.org
MESA(Mechatronics, Embedded Systems and Automation)LAB
School of Engineering, University of California, Merced, 5200 N Lake Road, Merced, CA 95343, USA

xuedingyu@ise.neu.edu.cn,
chendali@ise.neu.edu.cn
Information Science and Engineering
Northeastern University
Shenyang 110004, P R China

Conclusion

- Two fractional-order image segmentation model are proposed;
- The effective numerical algorithms are proposed;
- Improved accuracy;
- Provide a new tool for image segmentation.

Fractional Order Optical Flow

Introduction

What is the Optical Flow Problem?

Input: two or more frames of an image sequence;
Output: displacement field between two consecutive frames, optical flow.

What is Optical Flow Good for? [28-35]

- Robot navigation
- Tracking
- Action recognition
- Video compression
- Stereo reconstruction
- Medical image registration

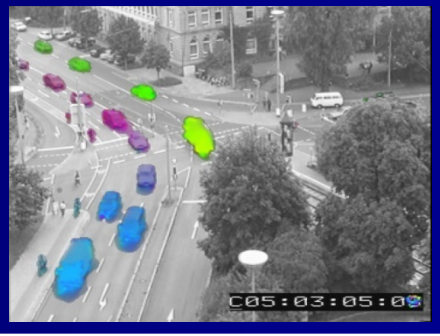

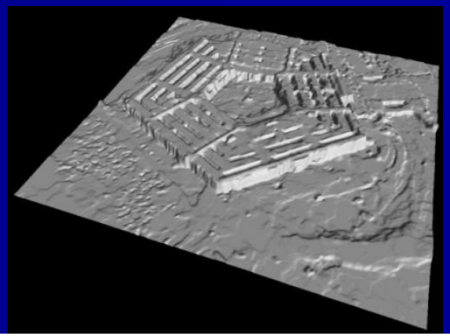

Fractional Order Optical Flow

Problem Description

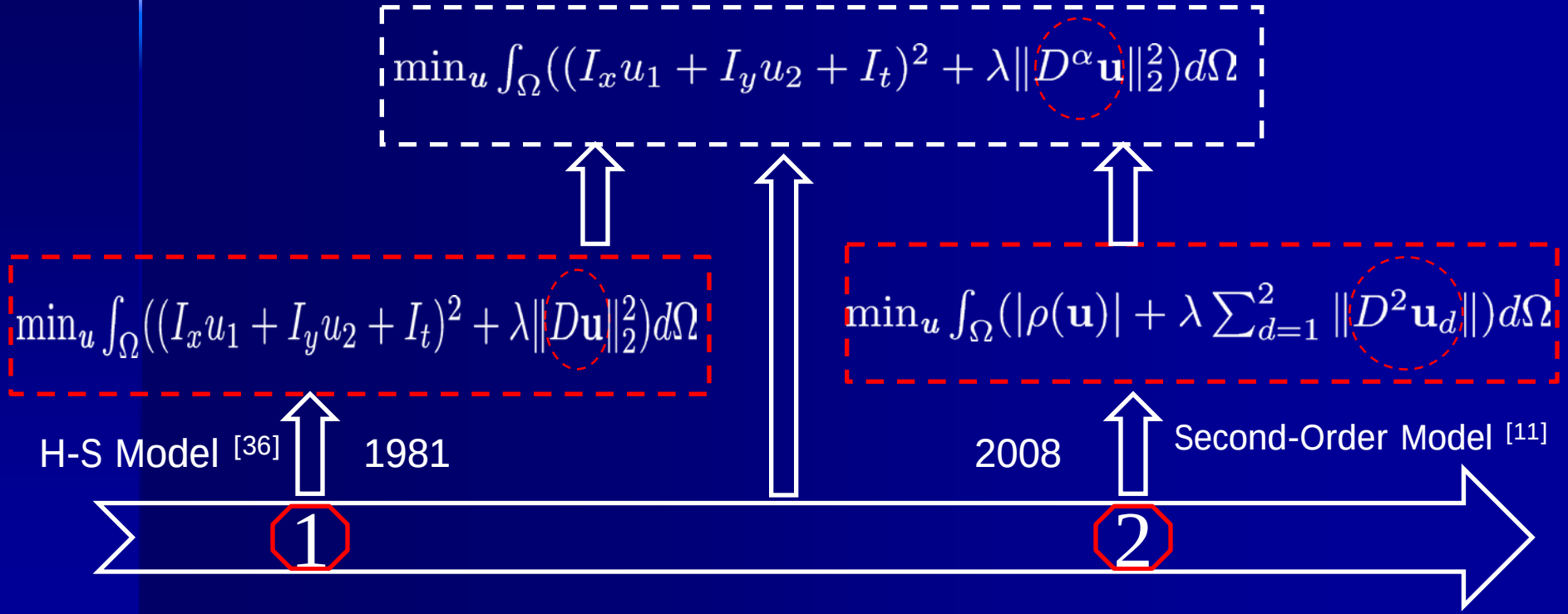

Outline

- Fractional-Order Optical Flow Model
- Numerical Algorithm
  - Euler–Lagrange Equation
  - Fractional-Order Differential Operator
  - Discrete Euler-Lagrange Equations
  - Structure of the Linear System
  - Multi-scale Approach
- Experiments

Outline

- Improved Fractional-Order Optical Flow Model
  - Discrete Formulation
  - Saddle-Point Formulation
- Numerical Scheme
- Experiments

Fractional-Order Variational Optical Flow Model [37]

Model description:

data term

regularization term

$$\min_{\boldsymbol{w}} \int_{\Omega} \left((I_x u + I_y v + I_t)^2 + \lambda \left(|D^{\alpha} u|^2 + |D^{\alpha} v|^2 \right) \right) d\Omega$$

$I_0(x, y, t)$ is the given image;

$(x, y)^T$ denotes the location with a rectangular image domain $\Omega \in R$;

$\boldsymbol{w}(x, y) := (u(x, y), v(x, y), 1)^{\top}$ is the optic flow field;

I_x, I_y and I_t are the gradients of image sequence I in x, y and t;

$D^{\alpha} := (D_x^{\alpha}, D_y^{\alpha})^{\top}$;

$|D^{\alpha} u| = \sqrt{(D_x^{\alpha} u)^2 + (D_y^{\alpha} u)^2}$.

Euler–Lagrange Equation

Consider an energy function J(u, v) defined by

$$J(u,v) = \int_\Omega ((I_x u + I_y v + I_t)^2 + \lambda(|D_x^\alpha u|^2 + |D_y^\alpha u|^2 + |D_x^\alpha v|^2 + |D_y^\alpha v|^2))d\Omega.$$

Assume that $u^*(x,y)$ and $v^*(x,y)$ are the desired functions. Take any test functions $\eta(x,y) \in C^\infty(\Omega)$ and $\zeta(x,y) \in C^\infty(\Omega)$ and $\epsilon \in R$.
We have

$$u(x,y) = u^*(x,y) + \epsilon\eta(x,y),$$
$$v(x,y) = v^*(x,y) + \epsilon\zeta(x,y).$$

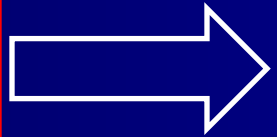

$$D_x^\alpha u(x,y) = D_x^\alpha u^*(x,y) + \epsilon D_x^\alpha \eta(x,y),$$
$$D_y^\alpha u(x,y) = D_y^\alpha u^*(x,y) + \epsilon D_y^\alpha \eta(x,y),$$
$$D_x^\alpha v(x,y) = D_x^\alpha v^*(x,y) + \epsilon D_x^\alpha \zeta(x,y),$$
$$D_y^\alpha v(x,y) = D_y^\alpha v^*(x,y) + \epsilon D_y^\alpha \zeta(x,y).$$

Euler–Lagrange Equation

$$J(\epsilon) = \int_\Omega ((I_x u^* + \epsilon I_x \eta + I_y v^* + \epsilon I_y \zeta + I_t)^2 + \lambda(|D_x^\alpha u^* + \epsilon D_x^\alpha \eta|^2 + |D_y^\alpha u^* + \epsilon D_y^\alpha \eta|^2 + |D_x^\alpha v^* + \epsilon D_x^\alpha \zeta|^2 + |D_y^\alpha v^* + \epsilon D_y^\alpha \zeta|^2))d\Omega. \quad (21)$$

Differentiating (21) with respect to ϵ, we obtain

$$J'(0) = \int_\Omega (\eta(MI_x + \lambda(D_x^{\alpha *} D_x^\alpha u^* + D_y^{\alpha *} D_y^\alpha u^*)) + \zeta(MI_y + \lambda(D_x^{\alpha *} D_x^\alpha v^* + D_y^{\alpha *} D_y^\alpha v^*)))d\Omega.$$

$$(I_x u^* + I_y v^* + I_t) I_x + \lambda(D_x^{\alpha *} D_x^\alpha u^* + D_y^{\alpha *} D_y^\alpha u^*) = 0,$$
$$(I_x u^* + I_y v^* + I_t) I_y + \lambda(D_x^{\alpha *} D_x^\alpha v^* + D_y^{\alpha *} D_y^\alpha v^*) = 0.$$

$D^{\alpha *}$ is the right Riemann-Liouville fractional derivative

Fractional-Order Differential Operator

Let: $w_0^{(\alpha)} = 1, \quad w_k^{(\alpha)} = (1 - \frac{\alpha+1}{k})\, w_{k-1}^{(\alpha)}, \qquad k = 1, 2, \ldots.$

We have: $D_x^{\alpha *} D_x^{\alpha} u(i,j) = \sum_{k=-\infty}^{0} w_{|k|}^{(\alpha)} u(i-k,j) + \sum_{k=0}^{\infty} w_k^{(\alpha)} u(i-k,j).$

Since $\sum_{k=0}^{\infty} w_k^{(\alpha)} = 0$, the equation can be rewritten by

$$D_x^{\alpha *} D_x^{\alpha} u(i,j) = \sum_{k=-\infty}^{-1} w_{|k|}^{(\alpha)} \nabla u(i-k,j) + \sum_{k=1}^{\infty} w_k^{(\alpha)} \nabla u(i-k,j), \quad (22)$$

where $\nabla u(i-k,j) = u(i-k,j) - u(i,j).$

Fractional-Order Differential Operator

For application, we approximate (22) using the following formula:

$$D_x^{\alpha *} D_x^{\alpha} u(i,j) \approx \sum_{k=-L}^{-1} w_{|k|}^{(\alpha)} \nabla u(i-k,j) + \sum_{k=1}^{L} w_k^{(\alpha)} \nabla u(i-k,j), \quad (23)$$

Similarly, we can obtain

$$D_y^{\alpha *} D_y^{\alpha} u(i,j) \approx \sum_{k=-L}^{-1} w_{|k|}^{(\alpha)} \nabla u(i,j-k) + \sum_{k=1}^{L} w_k^{(\alpha)} \nabla u(i,j-k). \quad (24)$$

Fractional-Order Differential Operator

From (23) and (24), the concise discrete formula of the fractional-order differential operator can be described by

$$D_x^{\alpha *} D_x^{\alpha} u(i,j) + D_y^{\alpha *} D_y^{\alpha} u(i,j) \approx \sum_{(\bar{i},\bar{j}) \in \chi(i,j)} w_{k_{\bar{i}\bar{j}}}^{(\alpha)} (u(\bar{i},\bar{j}) - u(i,j)),$$

$$D_x^{\alpha *} D_x^{\alpha} v(i,j) + D_y^{\alpha *} D_y^{\alpha} v(i,j) \approx \sum_{(\bar{i},\bar{j}) \in \chi(i,j)} w_{k_{\bar{i}\bar{j}}}^{(\alpha)} (v(\bar{i},\bar{j}) - v(i,j)).$$

$\chi(i,j)$ denotes the set of neighbors of pixel (i,j) in axis x and y;

$k_{\bar{i}\bar{j}}$ can be obtained by $max(|\bar{i} - i|, |\bar{j} - j|)$.

Discrete Euler-Lagrange Equations

Let: $I_{xx}(i,j) = I_x(i,j) \times I_x(i,j), \quad I_{yy}(i,j) = I_y(i,j) \times I_y(i,j),$

$I_{xy}(i,j) = I_x(i,j) \times I_y(i,j), \quad I_{tx}(i,j) = I_t(i,j) \times I_x(i,j),$

$I_{ty}(i,j) = I_t(i,j) \times I_y(i,j).$

The discrete Euler-Lagrange equations can finally be written as

$$I_{xx}(i,j)u(i,j)+I_{xy}(i,j)v(i,j)+\lambda \sum_{(\bar{i},\bar{j})\in\chi(i,j)} w^{(\alpha)}_{k_{\bar{i}\bar{j}}}(u(\bar{i},\bar{j})-u(i,j)) = -I_{tx}(i,j),$$

$$I_{xy}(i,j)u(i,j)+I_{yy}(i,j)v(i,j)+\lambda \sum_{(\bar{i},\bar{j})\in\chi(i,j)} w^{(\alpha)}_{k_{\bar{i}\bar{j}}}(v(\bar{i},\bar{j})-v(i,j)) = -I_{ty}(i,j).$$

(25)

Structure of the Linear System

The linear system can be written as: $AX = -B$

$$A = \begin{pmatrix} I_{xx} - \lambda D^{\alpha^*} D^{\alpha} & I_{xy} \\ I_{yx} & I_{yy} - \lambda D^{\alpha^*} D^{\alpha} \end{pmatrix}$$

$$X = [U, V]^T \qquad B = [I_{tx}, I_{ty}]^T$$

It can be solved by many typical methods such as the Jacobi method, the Gauß–Seidel method, the successive overrelaxation method and the preconditioned conjugate gradient (PCG) method.

Multi-scale Approach

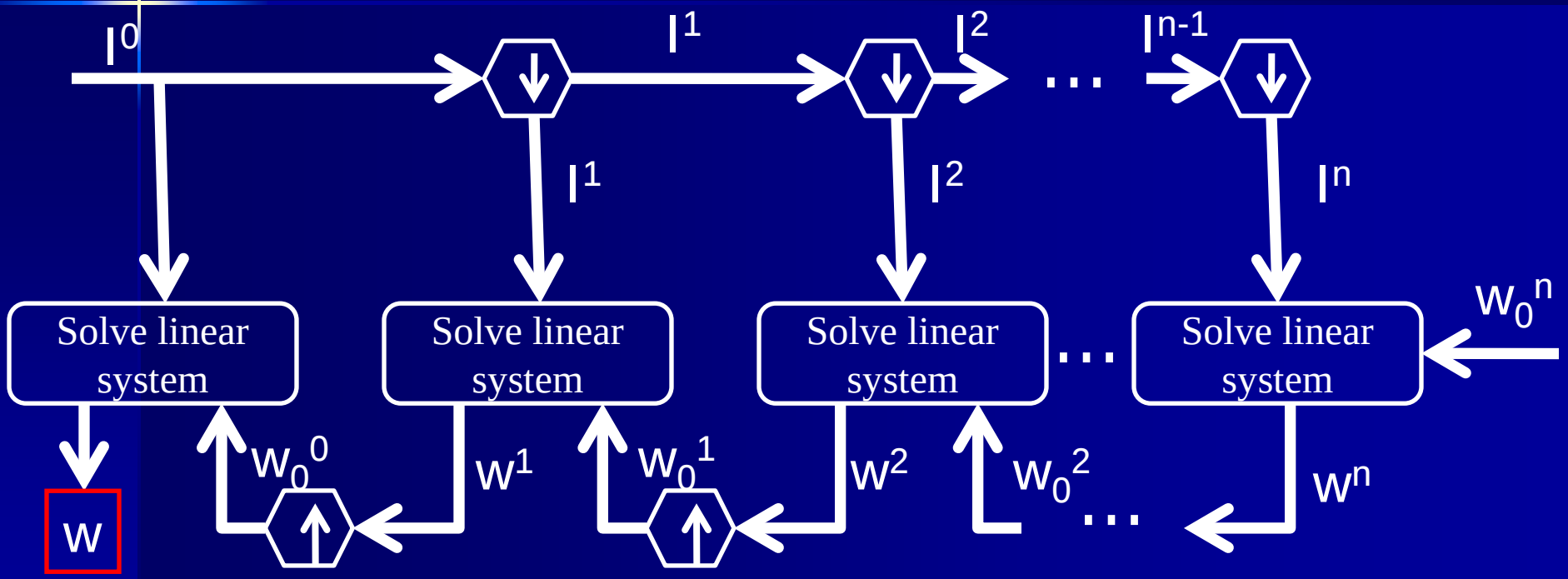

Good for finding the global minimum.

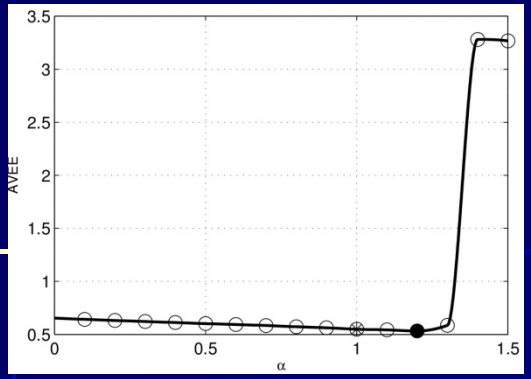

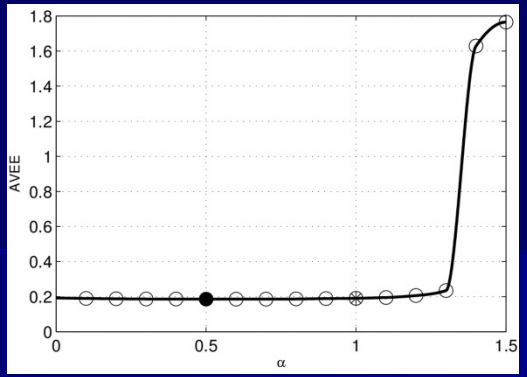

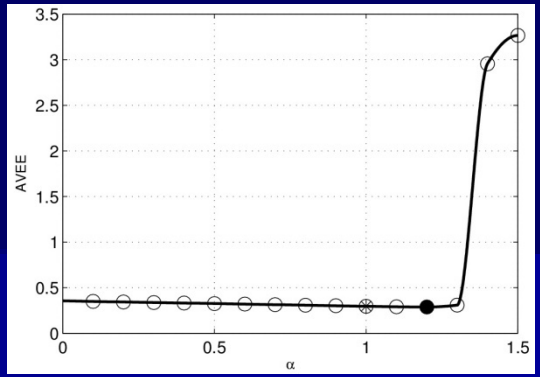

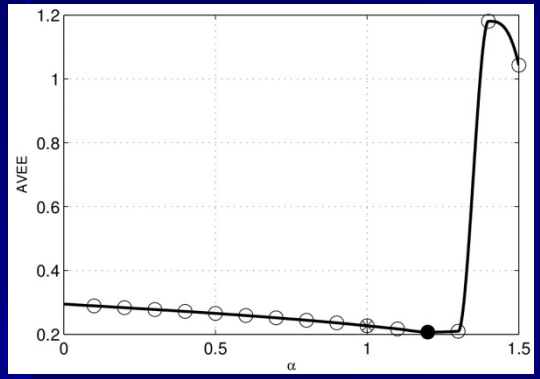

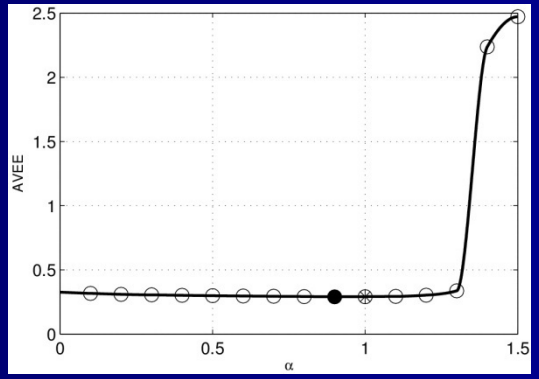

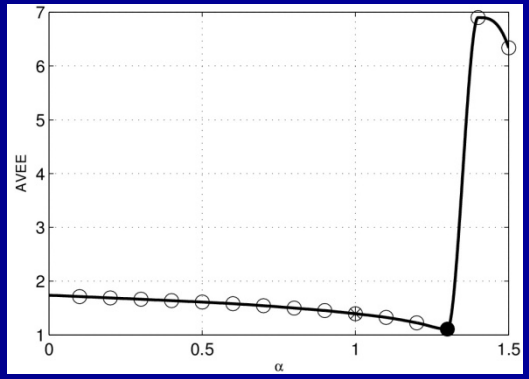

$$EE = \sqrt{(u - u_{GT})^2 + (v - v_{GT})^2}.$$

$(u, v, 1)$ is the estimated flow vector.

$(u_{GT}, v_{GT}, 1)$ is the ground-truth flow vector.

The accuracy of optical flow estimation algorithms can be improved by using the fractional-order derivative instead of the first-order derivative.

Image Sequence	Venus		
Models	AVAE	SDAE	AVEE
H-S model	0.1641	0.4176	0.5494
FOVOF model	**0.1561**	**0.3692**	**0.5334**
Image Sequence	Dimetrodon		
Models	AVAE	SDAE	AVEE
H-S model	0.0643	0.0638	0.1908
FOVOF model	**0.0617**	**0.0630**	**0.1861**
Image Sequence	Hydrangea		
Models	AVAE	SDAE	AVEE
H-S model	0.0522	0.1070	0.2967
FOVOF model	**0.0521**	**0.1063**	**0.2885**
Image Sequence	RubberWhale		
Models	AVAE	SDAE	AVEE
H-S model	0.1269	0.2588	0.2268
FOVOF model	**0.1167**	**0.2439**	**0.2071**
Image Sequence	Grove		
Models	AVAE	SDAE	AVEE
H-S model	0.0700	0.1321	0.2919
FOVOF model	**0.0696**	**0.1307**	**0.2910**
Image Sequence	Urban		
Models	AVAE	SDAE	AVEE
H-S model	0.2850	0.6526	1.3944
FOVOF model	**0.1865**	**0.4813**	**1.1085**

Comparison of AVAE, SDAE and AVEE between our proposed FOVOF model and H-S model for the different image sequences.

$$AE = \arccos\left(\frac{1+u\times u_{GT}+v\times v_{GT}}{\sqrt{1+u\times u+v\times v}\sqrt{1+u_{GT}\times u_{GT}+v_{GT}\times v_{GT}}}\right);$$

- From the table, it can be seen that our model obtains better results than the H–S model for all the image sequences.
- It demonstrates the validity of the generalization of differential order.

Improved Fractional-Order Variational Optical Flow Model

Model description:

$$\min_{g,w} \int_{\Omega} |D^{\alpha} g| + \int_{\Omega} c(|Dw|)|Dw| + \lambda \|\rho(w,g)\|_1 \qquad (26)$$

$\boldsymbol{w} := (u,v)^{\top}$ is the optic flow field;

g is the varying illumination;

$D^{\alpha} := (D_x^{\alpha}, D_y^{\alpha})^{\top}$; $\quad |D^{\alpha} u| = \sqrt{(D_x^{\alpha} u)^2 + (D_y^{\alpha} u)^2}$.

$$c(x) = \frac{1}{1 + (\frac{x}{\theta})^2}$$

Discrete Formulation

Discrete model:

$$\min_{g\in X, w\in Y} \|D^{\alpha} g\|_1 + \|c(|Dw|)Dw\|_1 + \lambda\|\rho(w,g)\|_1 \qquad (27)$$

$$\|c(|Dw|)Dw\|_1 = \sum_{i,j} c(|Dw_{ij}|)|Dw_{ij}| \quad \|D^{\alpha} g\|_1 = \sum_{i,j} |D^{\alpha} g_{ij}|$$

$$\rho(w,g) = I_t + (\nabla I)^T (w - w^0) + \beta g$$

$I(x,y,t)$ is the given image sequence;

$(x,y)^T$ denotes the location with a rectangular image domain $\Omega \in R$;

∇I is the spatial image gradient;

I_t is the time image gradient.

Saddle-Point Formulation

Saddle-Point Formulation: (28)

$$\min_{g\in X, w\in Y} \max_{p\in Y, q\in Z} \langle D^\alpha g, p\rangle_Y + \langle c(|Dw|)Dw, q\rangle_Z + \lambda\|\rho(w,g)\|_1 - \delta_P(p) - \delta_Q(q)$$

We define a scalar product in Y:

$$\langle a, b\rangle_Y = \sum_{i,j}(a_1 b_1 + a_2 b_2)_{ij} \quad a = (a_1, a_2) \in Y, \quad b = (b_1, b_2) \in Y$$

We define a scalar product in $Z = Y \times Y$:

$$\langle a, b\rangle_Z = \sum_{i,j}(a_1 b_1 + a_2 b_2 + a_3 b_1 + a_4 b_4)_{ij}$$

$$a = (a_1, a_2, a_3, a_4) \in Z, \qquad b = (b_1, b_2, b_3, b_4) \in Z$$

Saddle-Point Formulation

$$\delta_P(p) = \begin{cases} 0, & p \in P \\ +\infty, & others \end{cases} \qquad P = \{p \in Y : \|p\|_\infty \leq 1\}$$

$$\delta_Q(q) = \begin{cases} 0, & q \in Q \\ +\infty, & others \end{cases} \qquad Q = \{q \in Z : \|q\|_\infty \leq 1\}$$

Numerical Scheme

Step1:

Let the input image sequence be I and set $n = 0$.

Initialize w^0, g^0, p^0, q^0, α,λ, β, τ, σ and iteration number N_{iter}.

Step2:

$$p^{n+1} = \frac{\widetilde{p}^n}{\max(1, |\widetilde{p}^n|)} \qquad \widetilde{p}^{n+1} = p^n + \sigma D^\alpha \overline{g}^n$$

$$q^{n+1} = \frac{\widetilde{q}^n}{\max(1, |\widetilde{q}^n|)} \qquad \widetilde{q}^{n+1} = q^n + \sigma c(|D\overline{w}^n|) D\overline{w}^n$$

Step3:

$$g^{n+1} = \widetilde{g}^{n+1} + \begin{cases} \tau\lambda\beta, & \rho^{n+1} < -\tau\lambda|a|^2 \\ -\tau\lambda\beta, & \rho^{n+1} > \tau\lambda|a|^2 \\ -\frac{\rho^{n+1}\beta}{|a|^2}, & |\rho^{n+1}| \le \tau\lambda|a|^2 \end{cases}$$

$$w^{n+1} = \widetilde{w}^{n+1} + \begin{cases} \tau\lambda\nabla I, & \rho^{n+1} < -\tau\lambda|a|^2 \\ -\tau\lambda\nabla I, & \rho^{n+1} > \tau\lambda|a|^2 \\ -\frac{\rho^{n+1}\nabla I}{|a|^2}, & |\rho^{n+1}| \le \tau\lambda|a|^2 \end{cases}$$

$$\widetilde{g}^{n+1} = g^n - \tau D^{\alpha *} p^{n+1} \qquad \widetilde{w}^{n+1} = w^n - \tau c(|D^* q^{n+1}|) D^* q^{n+1}$$

$$|a| = \sqrt{\beta^2 + |\nabla I|^2} \qquad \rho^{n+1} = I_t + \nabla I(\widetilde{w}^{n+1} - w^0) + \beta\widetilde{g}^{n+1}$$

Numerical Scheme

Step4:

$$\overline{g}^{n+1} = 2g^{n+1} - g^n$$

$$\overline{w}^{n+1} = 2w^{n+1} - w^n$$

Step5:

If $n = N_{iter}$, stop; else, set $n = n + 1$ and go to step 2.

Multi-scale approach also is used.

Experiments: Venus

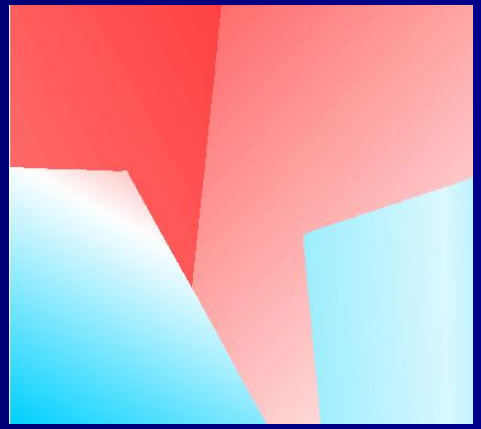

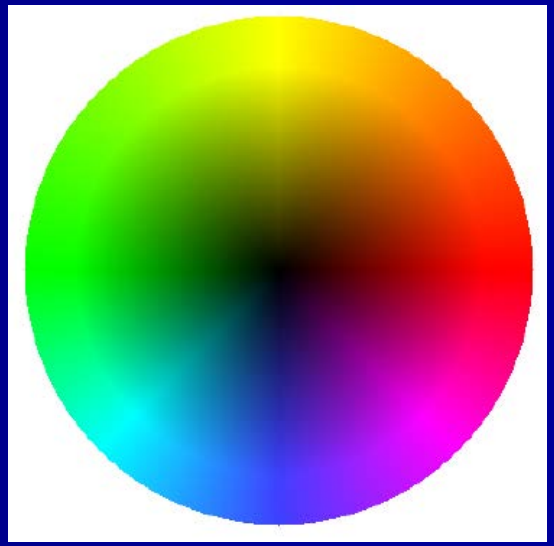

The test images come from [38]

Experiments: Venus

Fractional Order Optical Flow Demo: Venus

YangQuan Chen, Dali Chen, Dingyu Xue

yangquan.chen@ucmerced.edu;
yqchen@ieee.org
MESA (Mechatronics, Embedded Systems and Automation) LAB,
School of Engineering, University of California, Merced,
5200 N Lake Road, Merced, CA 95343, USA

chendali@ise.neu.edu.cn,
xuedingyu@ise.neu.edu.cn
Information Science and Engineering
Northeastern University
Shenyang 110004, P R China

Experiments: RubberWhale

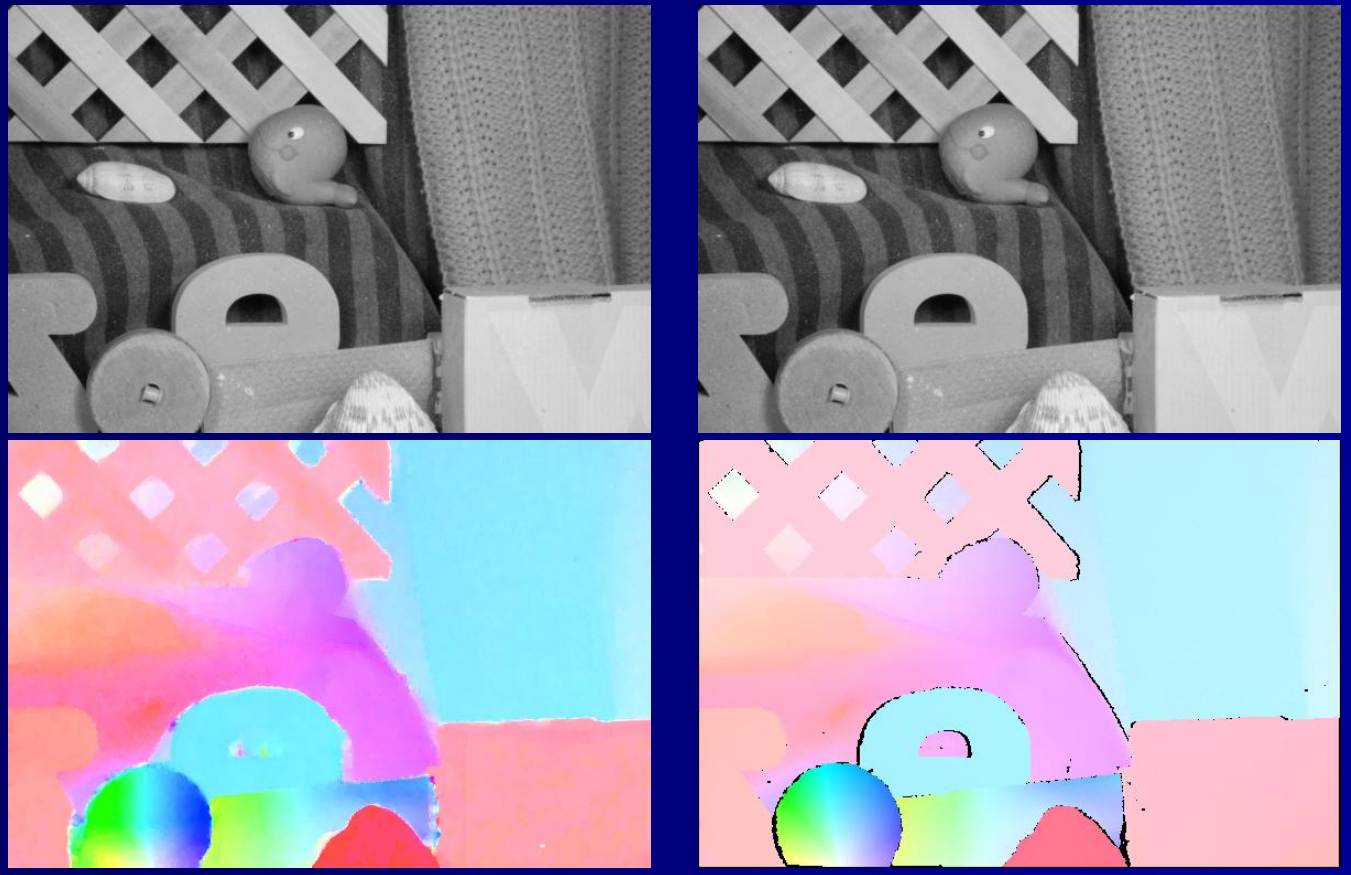

Experiments: RubberWhale

Fractional Order Optical Flow
Demo: RubberWhale

YangQuan Chen, Dali Chen, Dingyu Xue

yangquan.chen@ucmerced.edu;
yqchen@ieee.org
MESA (Mechatronics, Embedded Systems and Automation) LAB,
School of Engineering, University of California, Merced,
5200 N Lake Road, Merced, CA 95343, USA

chendali@ise.neu.edu.cn,
xuedingyu@ise.neu.edu.cn
Information Science and Engineering
Northeastern University
Shenyang 110004, P R China

Experiments: Hydrangea

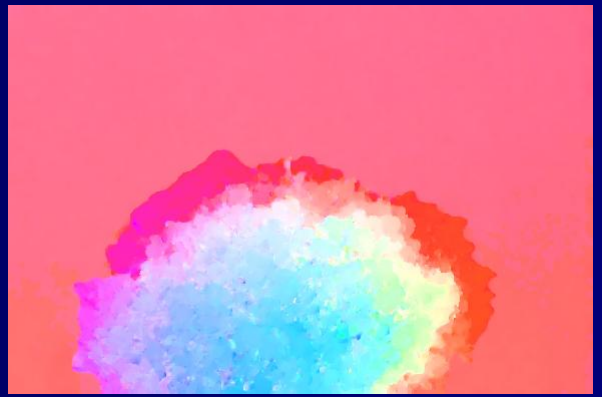

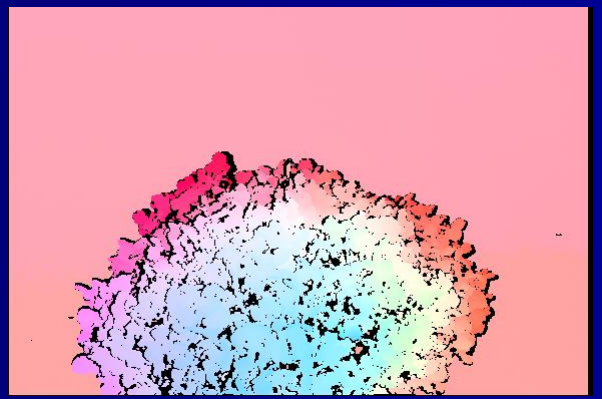

Experiments: Hydrangea

Fractional Order Optical Flow
Demo: Hydrangea

YangQuan Chen, Dali Chen, Dingyu Xue

yangquan.chen@ucmerced.edu;
yqchen@ieee.org
MESA (Mechatronics, Embedded Systems and Automation) LAB,
School of Engineering, University of California, Merced,
5200 N Lake Road, Merced, CA 95343, USA

chendali@ise.neu.edu.cn,
xuedingyu@ise.neu.edu.cn
Information Science and Engineering
Northeastern University
Shenyang 110004, P R China

Experiments: Grove

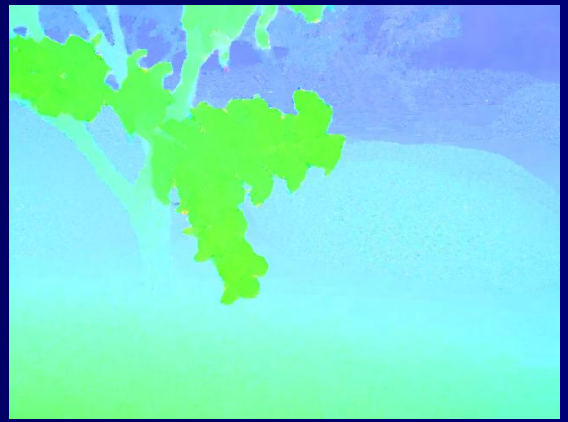

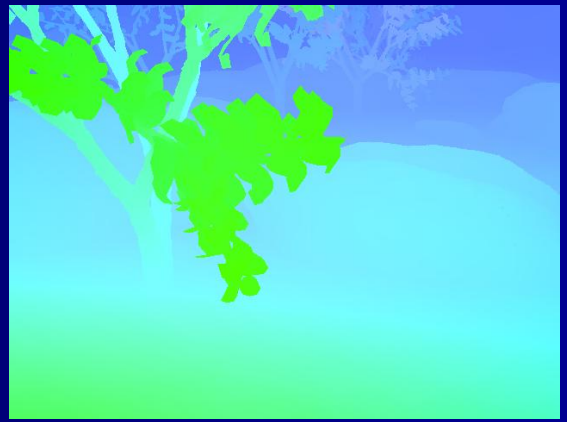

Experiments: Grove

Fractional Order Optical Flow
Demo: Grove

YangQuan Chen, Dali Chen, Dingyu Xue

yangquan.chen@ucmerced.edu;
yqchen@ieee.org
MESA (Mechatronics, Embedded Systems and Automation) LAB,
School of Engineering, University of California, Merced,
5200 N Lake Road, Merced, CA 95343, USA

chendali@ise.neu.edu.cn,
xuedingyu@ise.neu.edu.cn
Information Science and Engineering
Northeastern University
Shenyang 110004, P R China

Experiments: Dimetrodon

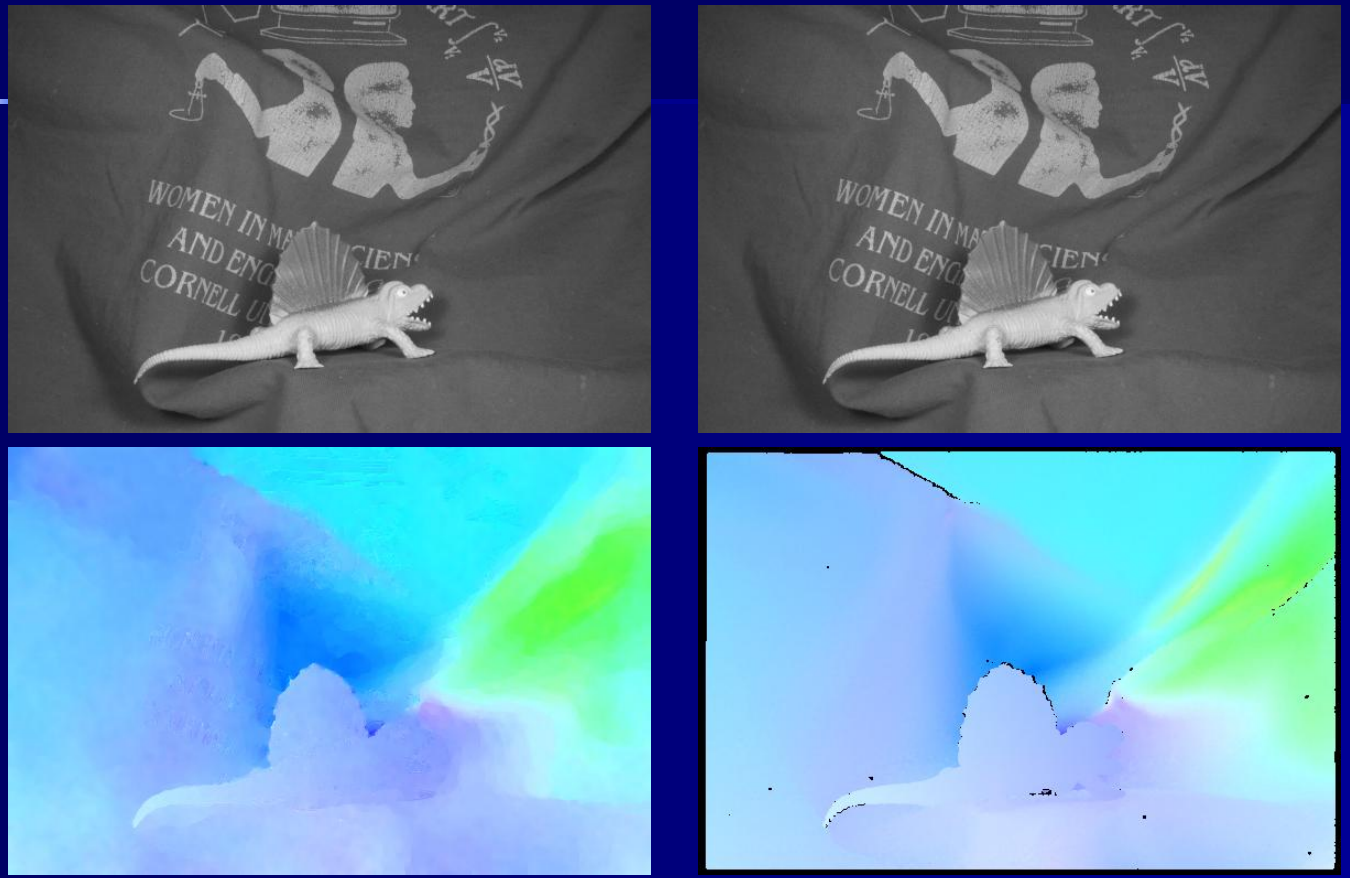

The proposed model is able to properly estimate the optical flow.

Experiments: Dimetrodon

Fractional Order Optical Flow
Demo: Dimetrodon

YangQuan Chen, Dali Chen, Dingyu Xue

yangquan.chen@ucmerced.edu;
yqchen@ieee.org
MESA (Mechatronics, Embedded Systems and Automation) LAB,
School of Engineering, University of California, Merced,
5200 N Lake Road, Merced, CA 95343, USA

chendali@ise.neu.edu.cn,
xuedingyu@ise.neu.edu.cn
Information Science and Engineering
Northeastern University
Shenyang 110004, P R China

The proposed model is able to properly estimate the optical flow.

Experiments:

Table 1: AVAE quantitative comparison

Model	Venus	Dimetrodon	Hydrangea	RubberWhale	Grove
H-S Model	0.1641	0.0643	0.0522	0.1269	0.0700
FOVOF Model	0.1561	0.0617	0.0521	0.1167	0.0696
IFOVOF Model($\alpha = 1$)	0.0875	0.0578	0.0401	0.0718	0.0478
IFOVOF Model($\alpha = 1.2$)	0.0869	0.0567	0.0393	0.0695	0.0476

- This model obtains better results than the FOVOF model.
- The generalization of differential order is helpful for improving the accuracy.

Conclusion

- Two fractional-order variational optical flow model are proposed, see in [37];
- Two effective numerical algorithms are proposed;
- They can be combined with the multi-scale approach;
- Improve the accuracy;
- Provide a new tool for motion estimation.

Reference List

1. Gonzalez, R.C., Woods, R.E.: Digital Image Processing. Prentice Hall, New Jersey (2002)
2. Dali Chen, YangQuan Chen* and DingyuXue. “Digital Fractional Order Savitzky-Golay Differentiator.” IEEE Trans. Circuit and Systems II, Volume: 58 Issue: 11 Pages: 758-762 Published: NOV 2011, DOI: 10.1109/TCSII.2011.2168022
3. Dali Chen, YangQuan Chen, DingyuXue. 1-D and 2-D digital fractional-order Savitzky-Golay differentiator. Signal, Image and Video Processing 05/2012; 6(3):503-511. DOI 10.1007/s11760-012-0334-0
4. B. Mathieu, P. Melchior, A. Oustaloup, and C. Ceyral, Fractional differentiation for edge detection," Signal Process., vol. 83, pp. 2421-2432,November 2003.
5. I. Podlubny, Ed., Fractional Di®erential Equations. San Diego: Academic Press, 1999.
6. Dali Chen, DingyuXue, YangQuan Chen. “Fractional differentiation-based approach for robust image edge detection” (#046) Proceedings of 2012 Fractional Derivative and Applications (FDA2012), Nanjing, China, May 15-17, 2012.

Reference List

7. P. Perona and J. Malik, “Scale-space and edge detection using anisotropic diffusion,” IEEE Transactions on Pattern Analysis and Machine Intelligence, vol. 12, no. 7, pp. 629–639, 1990.
8. Y. L. You and M. Kaveh, “Fourth-order partial differential equations for noise removal,” IEEE Transactions on Image Processing, vol. 9, no. 10, pp. 1723–1730, 2000.
9. L. Ruding, S. Osher, E. Fatemi, Physica D. 60, 259 (1992)
10. B. Jian and X. C. Feng, “Fractional-order anisotropic diffusion for image denoising,” IEEE Transactions on Image Processing, vol. 16, no. 10, pp. 2492–2502, 2007.
11. W. Trobin, T. Pock, D. Cremers, and H. Bischof. An unbiased second-order prior for high-accuracy motion estimation. DAGM 2008.
12. Dali Chen, Shenshen Sun, Congrong Zhang, YangQuan Chen, DingyuXue. Fractional-Order TV-L2 Model for Image Denoising. 2013. Special Issue on "Fractional Calculus: Theory and Numerical Methods” http://www.springerlink.com/openurl.asp?genre=article&id=doi:10.2478/s11534-013-0241-1 (Central European Journal of Physics) (online)

Reference List

13. P. Guidotti, J. V. Lambers, J. Math Imaging Vis. 33, 25 (2009)
14. E. Cuesta, M. Kirane, S. A. Malik, Signal Processing. 92, 553 (2012)
15. M. Janev, S. Pilipovi c, T. Atanackovi c, R. Obradovi c, N. Ralevi c, Mathematical and Computer Modelling.54, 729 (2011)
16. Y. Wang, W. Yin, and Y. Zhang, A Fast Algorithm for Image Deblurring With Total Variation Regularization, Rice Univ., Houston. TX,Tech. Rep., 2007
17. M. A. T. Figueiredo, J. M. Bioucas{Dias, R. D. Nowak, IEEE Transactions on Image Processing. 16, 2980(2007)
18. J. P. Oliveira, J. M. Bioucas{Dias, M. A. T. Figueiredo, Signal Processing. 89, 1683 (2009)
19. M. Hajiaboli, IPSJ Transactions on Computer Vision and Application. 2, 94 (2010)
20. T.F. Chan, L.A. Vese. Active contours without edges [J], IEEE Transactions on Medical Imaging, 2001, 10 (2): 266-277.
21. Li Chunming, Kao Chiu-Yen, Gore John C.. Ding Zhaohua. Minimization of region-scalable fitting energy for image segmentation [J], IEEE Transactions on Image Processing, 17(10): 1940-1949.2008

Reference List

22. D. Adalsteinsson, J. Sethian. A Fast Level Set Method for propagating interface [J], Journal of Computational Physics,1995,118: 269-277.
23. D. Mumford, J. Shah. Boundary detection by minimizing functions. IEEE Computer Society Conference on Computer Vision ans Pattern Recognition, San Francisco, CA, USA, 1985: 22-26.
24. C. Li, C. Xu, C. Gui, M. D. Fox. Level set evolution without re-initialization: A new variational formulation. IEEE Conference on Computer Vision and Pattern Recognition(CVPR), 2005, 1: 430-436.
25. S.Osher, J.A.Sethian. Fronts propagating with curvature dependent speed: algorithm based on Hamilton-Jacobi formulation[J]. Journal of Compute Physics, 1988, 79(1): 12-49.
26. Zhao H K, Chan T, Merriman V. A variational level-set approach to multiphase motion[J]. Journal of Computational Physics, 1996, 127(1):179-195
27. Sapiro G. Geometric partial differential equations and image analysis[M]. Cambridge University Press, 2001.

Reference List

28. T. Brox and J. Malik. Large displacement optical flow: descriptor matching in variational motion estimation. PAMI 33(3):500-513, 2011.
29. T. Brox, A. Bruhn, N. Papenberg, and J. Weickert. High accuracy optical flow estimation based on a theory for warping. ECCV 2004.
30. H. Zimmer, A. Bruhn, J. Weickert, L. Valgaerts, A. Salgado, B. Rosenhahn, and H.-P. Seidel. Complementary optic flow. EMMCVPR 2009.
31. P. Gwosdek, H. Zimmer, S. Grewenig, A. Bruhn, and J. Weickert. A highly efficient GPU implementation for variational optic flow based on the Euler-Lagrange framework. CVGPU Workshop 2010.
32. T. Brox, A. Bruhn, N. Papenberg, and J. Weickert. High accuracy optical flow estimation based on a theory for warping. ECCV 2004.
33. H. Zimmer, A. Bruhn, J. Weickert. Optic flow in harmony. IJCV 93(3) 2011.
34. S. Volz, A. Bruhn, L. Valgaerts, and H. Zimmer. Modeling temporal coherence for optical flow. ICCV 2011.

Reference List

35. M. Stoll, A. Bruhn, and S. Volz. Adaptive integration of feature matches into variational optic flow methods. ACCV 2012.
36. Horn B, Schunck, B. 1981 Determining optical flow. Artif. Intell. 16, 185–203. (doi:10.1016j.bbr.2011.03.031)
37. Dali Chen, Hu Sheng, YangQuan Chen and DingyüXue. Fractional-order variational optical flow model formotion estimation. Phil Trans R Soc A 20120148. http://dx.doi.org/10.1098/rsta.2012.0148 (proofread, to appear)
38. Simon B, Daniel S, Lewis JP, Stefan R, Michael JB, Richard S. 2011 A database and evaluation methodology for optical flow. Int. J. Comput. Vis. 92, 1–31. (doi:10.1007/s11263-010-0390-2)
39. Chambolle A, Pock T. A first-order primal-dual algorithm for convex problems with applications to imaging[J]. J Math Imaging Vis, 2011, 40(1): 120-145.

Take home message:

More optimal image processing can be made possible by using fractional order differentiation and fractional order partial differential equations.

Want to be more optimal? Go fractional calculus!

Q & A

More info:

http://mechatronics.ucmerced.edu/research/applied-fractional-calculus